COST-EFFECTIVE AND HIGH-PERFORMANCE DYE-SENSITIZED SOLAR CELLS USING POLYMER-BASED COUNTER ELECTRODES

Sherif Dei Bukari
Bachelor of Science in Chemistry

Submitted in fulfillment of the requirements for the degree of Master of Science in Chemistry

School of Sciences and Humanities
Department of Chemistry
Nazarbayev University

53 Kabanbay Batyr Avenue,
Nur-Sultan, Kazakhstan,
010000

Supervisor: Mannix P. Balanay, PhD

Co-supervisor: Bakhytzhan Baptayev, PhD

April 2023

Abstract

Solar energy has proven to be the most promising solution to the current and future world energy and environmental challenges. One of the most promising technologies to harvest solar energy is the dye-sensitized solar cell (DSSC) due to its eco-friendliness, affordability, high efficiency, good durability, and simple manufacturing processes. An expensive platinum electrode is one of the major limitations of DSSCs. Here we fabricate a cheaper and more effective counter electrode based on Poly(3,4-ethylene dioxythiophene) and N-alkyl carbazole derivatives (N-butyl-, N-hexyl-, and N-octyl carbazole) copolymers (PEDOT-CO-RCbz) as better substitutes for the traditional platinum counter electrode via a simple electrochemical deposition method. The fabricated PEDOT and PEDOT-CO-RCbz counter electrodes have a highly porous sponge-like morphology with lower charge-transfer resistance and higher electrocatalytic activity for catalyzing the iodine/triiodide redox reaction than the classical Pt electrodes. The DSSCs with PEDOT-CO-RCbz counter electrodes all have better power conversion efficiency (the highest being 8.88%) than the DSSC with only PEDOT (7.9%) and Pt (~7.6%) counter electrodes. The superior photoelectric characteristics, a straightforward preparation process, and a low cost make PEDOT-CO-RCbz counter electrodes promising substitutes for DSSCs.

Acknowledgments

All praises be upon Allah, the most gracious, the especially merciful. I would like to first thank Allah for the lives and health of the workers, students, and lecturers at Nazarbayev University.

I would like to also express my heartfelt gratitude to my research supervisor, Dr. Mannix Balanay, and co-supervisor, Dr. Bakhytzhan Baptayev, for their patience and relentless guidance that has helped me sail through my studies at Nazarbayev University. I am also very grateful to all the members of the fmc^2 laboratory, especially Dr. Yerbolat Tashenov, Enoch Adotey, Ayagoz Ibrayeva, and Diana Suleimenova, for creating such a conducive atmosphere that has promoted a cohesive workforce and optimal working conditions.

I also acknowledge my supervisory committee for guiding me through my thesis work, and the Master's Chemistry program director at NU, Dr. Andrey Khalimon, for his guidance as well.

Finally, I am very grateful to my loving family for their care and motivation.

Table of Contents

Abbreviations

DMSO	*Dimethylsulfoxide*
$LiCl_4$	*Lithium per chlorate*
DSSC	*Dye-sensitized solar cell*
DSC	*Dye solar cell*
NMR	*Nuclear Magnetic Resonance*
UV	*Ultraviolet*
Vis	*Visible*
Cbz	*Carbazole*
PCbz	*Polycarbazole*
PEDOT	*Poly(3,4-ethylenedioxythiophene)*
EDOT	*3,4-ethylenedioxythiophene*
Cbz-C8	*Octyl carbazole*
Cbz-C6	*Hexyl carbazole*
Cbz-C4	*Butyl carbazole*
PV	*Photovoltaic*
CE(s)	*Counter electrode(s)*
TCO	*Transparent conducting oxide*
TBU_4PF_6	Tetrabutylammonium hexafluorophosphate

List of Figures

1 Introduction

1.1 Background study

The increasing global demand for energy and humanity's dependence on fossil fuels have hastened the depletion of Earth's oil reserves [1-3]. Consequently, the use of fossil fuels has led to serious environmental pollution and ecological changes like global warming [1-4]. Renewable energy sources have been considered the best way to alleviate the current energy crisis [1]. Thus, renewable energy storage and development has received a lot of attention worldwide due to the need to find replacements for fossil fuels [2]. It is expected that the energy demand will reach 50TW in the next 3 decades [6]. Some of the promising renewable and clean energy sources include solar energy, geothermal, wind, hydropower, and biomass [5]. Researchers are particularly interested in solar energy because of the enormous amount of energy that the sun provides to the earth each year (~3×10^{24} J), which is 10,000 times more energy than the world's population consumes [1-6]. In addition solar energy is considered one of the most promising sources of renewable energy as it is a more economical and clean form of energy [2]. Photovoltaic (PV) cells, or solar cells, are known to be the most suitable ways to efficiently convert solar energy directly into electrical energy [2-3], and covering 0.1% of the planet's surface with solar cells that have a power conversion efficiency (PCE) of at least 10% will be enough to meet the world's energy needs [31].

The dye-sensitized solar cell (DSSC), after its invention in 1991 by O'Regan and Grätzel, has attracted a lot of attention among other third-generation solar cells over the last three decades [7-9]. This is due to its relatively low cost, easy fabrication methods, and high efficiency [10, 11]. The DSSC is a two electrode electrochemical cell that typically consists of a semiconductor, counter electrode (CE), electrolyte, and dye-sensitizer that are sourced from titanium dioxide (TiO_2), platinum (Pt), tri-iodide/iodide, and ruthenium-based dyes like N719, respectively. A low-cost, high-efficiency DSSC using colloidal TiO_2 as the photoanode was able to reach ~7.1–7.9% PCE in simulated solar light, according to O'Regan and Grätzel [31]. Despite the fact that DSSCs have achieved PCE up to 10% under AM 1.5 (100 mW/cm2) [32], the commercialization of DSSC are still constrained by the costly and scarce Pt used as a CE. In order to find substitutes for the Pt

CE, this study will concentrate on fabricating a relatively cheaper CE based on copolymers of two common conducting polymers, since one (N-alkyl carbazole derivative) enhances the catalytic ability of the other (EDOT).

1.2 Problem statement

Pt is met with various limitations such as its scarcity, requirement for high-temperature processing, corrosion when in contact with electrolyte as well as its high cost [13]. Thus, our research group is focused on developing a new CE material with promising qualities like high conductivity, high surface area, and high availability, which can enhance the efficiency, electrocatalytic activity, and especially lower the overall cost of the DSSC serving as a suitable replacement for the Pt CE. This study will take advantage of relatively cheap and abundant monomers such as 3,4-ethylenedioxythiophene (EDOT) and N-alkyl derivatives of carbazole (RCbz), to fabricate poly(EDOT-Co-RCbz)-based CEs that are cost-effective and promising candidates for replacing the Pt CE. Polycarbazole possesses desirable conductivity and high surface area, but readily dissolves when exposed to the tri-iodide/iodide electrolyte. N-alkyl substituents increases the stability of Cbz, and copolymerizing EDOT with Cbz yields stable CEs and DSSC devices with higher PCE than a DSSCs based on only PEDOT. Our research group, fmc^2, is then focused on employing simple anodic electrochemical polymerization to fabricate poly(EDOT-Co-RCbz) counter electrodes for catalyzing the tri-iodide/iodide redox reactions.

1.3 Objectives of research

In this study, we aim to:

1. To fabricate poly(EDOT-Co-RCbz) as a counter electrode for DSSC via anodic electrochemical polymerization.
2. To investigate the effect of PEDOT electropolymerized with various derivatives of polycarbazole (PCbz) as counter electrodes on the DSSC performance.
3. To characterize the fabricated counter electrode using SEM, CV, EIS, J- V, and UV-vis analysis.

This thesis work is structured as follows: Chapter 2 consists of a brief literature survey that describes the general structure of a DSSC, highlights some of the most utilized conducting

polymers as counter-electrode materials, factors influencing their catalytic properties, ways to enhance these CEs, as well as some of the widely employed characterization methods. Chapter 3 describes the experimental part of this thesis providing the various methods used for this work. The results obtained are discussed and presented in Chapter 4. Chapter 5 includes the conclusion and future work.

2 Literature Review

2.1 Basic structure of DSSCs

The traditional DSSC is generally composed of a transparent conducting oxide like the fluorine-doped tin oxide (FTO) as substrate, a photoanode (consisting of a semiconductor and a dye sensitizer), an electrolyte containing a redox couple, and a counter electrode [10]. The basic working principle of DSSC begins with the photoexcitation of the dye which leads to the injection of an electron into the conduction band of the semiconductor, thereby oxidizing the dye [2]. Flowing through the semiconductor, the injected electron travels via the conductive substrate, such as transparent conductive oxides, and into the external circuit [2, 4]. The redox couple contained in the electrolyte then regenerates the dye restoring it to the ground state [2-4]. Electron transfer from the counter electrode in turn regenerates the oxidized redox couple, catalyzing the redox reduction in the electrolyte [2-5]. The fundamental processes via which DSSCs convert light energy into electrical energy can be summarized into 5 steps (**1-5**) as depicted in **Figure 1**. These include photoexcitation by sensitizer to produce excited dye (step 1); injection of an electron into the conduction band of the semiconductor to yield oxidized dye (step 2); transfer of electron to anode and through the external circuit to the counter electrode (step 3); transfer of electrons from redox couple to sensitizer resulting in oxidized dye regeneration (step 4); regeneration of oxidized redox couple via accepting electrons transferred from the counter electrode (step 5) [3]. Thus, all three components play vital roles in directly converting solar energy to electrical energy [1].

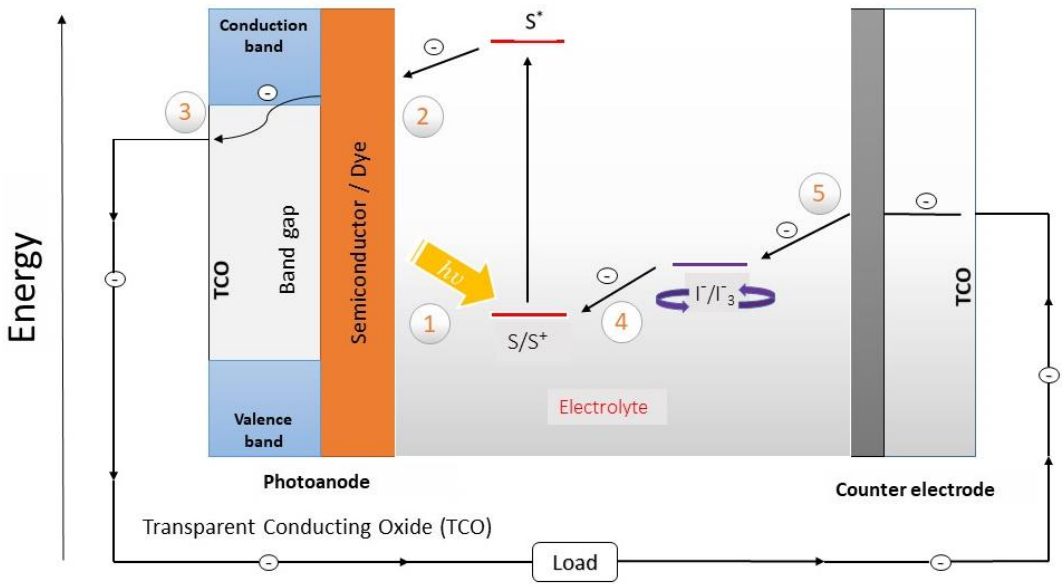

Figure 1. Basic processes and components of a dye-sensitized solar cell.

The most commonly employed semiconductor is titanium oxide (TiO_2) [1-5]. DSSC device based on TiO_2 semiconductor, fabricated by Grätzel, achieved a power conversion efficiency of about 7% [1]. Subsequent modifications to the TiO_2 semiconductor (Nanoparticle-haze, Nano-embossed hollow spheres, TiO_2–SiO_2 composite, doping with 1% Y^{3+}, optimizing the amount of Ho^{3+}-Yb^{3+}-F^{-} tri-doped TiO_2/pure TiO_2) have achieved a certified efficiency up to 11% [21-25]. Many promising competitors like ZnO [26], SnO_2 [27], Fe_2O_3 [28], Nb_2O_5, Ta_2O_5, and $SrTiO_3$ [29], have risen in past decades challenging titanium oxide as the semiconductor material for DSSCs [1]. However, TiO_2-based semiconductors are still considered the best options as they yield higher efficiencies [30].

Similarly, several dyes have been developed and employed as sensitizers over the past decades. These include dyes based on Ruthenium complexes, Osmium complexes, abundant metal complexes, porphyrin dyes, and metal-free organic dyes [12]. Metal-based dyes and organic dyes have drawn a lot of attention among the most commonly employed dyes in DSSCs due to their superior performance over other dyes [12]. Ruthenium (Ru)-based dyes have been the most common sensitizers employed in DSSC after its first design 3 decades ago, which achieved a power conversion efficiency of about 7% [12, 31]. Later, newly synthesized and modified Ru-based

sensitizers, yielding dyes like N749 and N719, achieved higher efficiencies of approximately 11% [12, 32–35]. Ru-based dyes are known for their feasible practical applications due to their desirable photo-electrochemical properties and stable redox states [36]. Although ruthenium-based dyes are promising sensitizers for DSSCs, not only is Ru toxic, but also less abundant on Earth [12, 37]. This has therefore prompted researchers to look for alternative dye materials that are less toxic, more effective, and abundant [12]. Research development addressing other metals has shown that there are promising alternatives including both rare and abundant metals [12]. But more recently, metal-free organic dyes for DSSC applications are increasingly garnering a lot of attention (as compared to metal-based dyes) due to their cost effectiveness, high molar extinction coefficients, simple preparation methods, and stability in high-temperature conditions [38]. Despite the tremendous work and efforts that have been put into developing and improving organic dyes as sensitizers for DSSC applications (both experimentally and computationally), only a hand full of metal-free organic dyes have achieved efficiencies comparable to metal-based dyes [12, 39-41]. Moreover, the photosensitizers do not contribute significantly to the total cost of the DSSC device [43], as the dye loading capacity of a DSSC is about 3×10^{-7} mol cm^{-2} [42]. This implies that for a Ru-based photosensitizer like the N719, only 0.35 mg cm^{-2} is needed [42]. This, therefore, renders the need to replace the metal-based dyes with more sustainable alternatives relatively less urgent in terms of reducing the cost of the DSSC device [43].

Even though the lifetime of the DSSC is generally influenced by several factors such as the removal of adsorbed dye on the TiO_2 surface, corrosion of counter electrode by the redox mediator, leakage of electrolytes, and electrolyte bleaching, the durability of the device is largely affected by the electrolytes that are employed [43]. The most commonly utilized electrolyte for DSSC is the iodine redox couple (I^-/I_3^-) [43]. The traditional iodine redox couple is prone to degradation issues and possesses a corrosion-inducing effect on counter electrodes leading to short-term stability [43]. Researchers have developed different alternative routes as a solution to the traditional iodine-based electrolyte issues [44]. Alternatives to the conventional I^-/I_3^- redox mediator that are less susceptible to evaporation; such as solid-state polymer-based electrolytes [43, 44], ionic liquids [45], and even aqueous-based electrolytes have been explored [46]. Even though these alternatives promise good stability and low toxicity, they provide lower efficiencies [47]. Meanwhile, recently explored cobalt-based redox mediators serve as the best alternatives to iodine-based redox mediators, offering a high efficiency up to 13% [48]. However, the toxicity of

cobalt and political challenges associated with its supply, places a limitation on employing cobalt as an electrolyte for DSSC [43, 48, 49]. For these reasons, iodine-based electrolyte remains the most common choice among researchers [12, 43].

The photoanodes and electrolytes of DSSCs have been explored to a larger extent, and seem to have a limited range of options as compared to the counter electrodes [1]. As briefly mentioned in the previous section, the counter electrode of the DSSC collects electrons from the external circuit to reduce the oxidized redox couple in the electrolyte. An electrocatalyst exhibiting low internal impedance to electron transfer displays greater catalytic activity reduction towards the redox couple, as well as a high fill factor (FF) [2]. Factors such as the sheet resistance of the transparent conducting oxide (TCO), transparency, and TiO_2 charge transfer resistance all contribute significantly to high efficiency in the counter electrode [2]. For a 550 nm wavelength, transparency should be greater than 80%, the sheet resistance should be less than 20 Ω^{-2}, and the charge transfer resistance should be within the range of 2-3 Ω cm^{-2} to achieve a CE with high performance [88]. Several research investigations have been devoted to replacing the Pt-based counter electrodes with cheaper alternatives, and polymer-based counter electrodes have emerged as promising alternatives. The advancements in the application of conducting polymers as electrocatalysts for DSSCs are further discussed in the following section.

2.2 Conducting polymers as counter electrodes for DSSCs

The discovery of conducting polymers, specifically intrinsic conducting polymers, was made in 1977 by Shirakawa, MacDiarmid, and Heeger [52, 53]. CPs belong to the fourth generation of polymers, and their development has progressed from laboratory materials to several industrial products and applications. This discovery received a Nobel Prize in 2000 [53, 54]. Organic polymers that are capable of conducting electricity like metals or as semiconductors due to their conjugated double bonds are considered conducting polymers [3]. CPs are generally advantageous as materials for a wide range of applications due to their fine-tunability via methods of organic synthesis, as well as their easy processability [3]. Polythiophenes, polypyrrole, or polyacetylene are some of the most common conducting polymers from which other derivatives are obtained [3].

Conducting polymers are considered promising CE materials due to their good conductivity, abundance, porous structures, and favorable electrocatalytic activity [3]. Furthermore, the applicability of CPs as CE materials is favored by the affordability and feasibility of their synthesis [3]. Various conducting polymers such as PANI, PPy, PEDOT, etc., and their composites or copolymers have been extensively investigated as cost-effective CE materials in Pt-free DSCs [1-3, 51, 53]. This section briefly surveys some of the most promising polymer-based counter electrodes fabricated for catalyzing the electrolytes in dye-sensitized solar cells.

2.2.1 Poly(3,4-ethylenedioxythiophene)

In the late 19th century, Poly(3,4-ethylenedioxythiophene) (PEDOT) was derived for the first time at the Bayer Lab [56, 57]. PEDOT exhibited superior conductivity (300–500 S cm^{-1}) to that of polypyrrole, polythiophene, and polyaniline [55]. Although the application of PEDOT was limited by its poor solubility, doping with poly(styrene sulfonate) (PSS) remedied this issue [58]. Due to its favorable features such as high conductivity, excellent transparency in visible light, and good stability, PEDOT has had various applications as a promising material for electronics, antistatic, and optoelectronics [59, 60].

PEDOT was first investigated as a counter electrode for dye-sensitized solar cells in 2002 by Saito and co-researchers-taking advantage of the high conductivity, catalytic activity, electrochemical reversibility, and favorable thermal and chemical stability of PEDOT- via the chemical polymerization of EDOT monomer on fluorine-doped tin oxide (FTO) [61]. The same authors put in efforts to improve the catalytic ability of PEDOT in reducing the redox mediators in DSSCs by doping PEDOT with p-toluenesulfonate (TsO) and polystyrene sulfonate (PSS) [3, 61]. The DSSC device with PEDOT-TsO CE displayed a power conversion efficiency (PCE) approximately the same as that of the device with Pt CE, and better than that of the cell with PEDOT-PSS CE [61]. The authors suggested that the lower efficiency of the cell with PEDOT-PSS CE is due to an increase in overpotential as a result of exposure to PSS [61]. In another work, Pringle et al. [62] electrodeposited PEDOT films on a flexible conducting substrate within a rapid deposition time of 5 seconds achieving a highly efficient and transparent PEDOT film. The obtained PEDOT film yielded a high PCE of 8.0% [62].

Structural characterization and studies indicate that the morphology of counter-electrode materials often plays an essential role in their effectiveness in catalyzing the electrolyte of the DSSCs [3]. The electrochemical properties of PEDOT and the photovoltaic performance of a DSSC device are found to be influenced by the morphology of PEDOT [3]. Given this, Ahmad and coworkers successfully fabricated nanoporous layers of PEDOT on an FTO substrate via electro-oxidative polymerization in the medium of hydrophobic ionic liquids as a way to modify the nanoporous structure via process control [63]. The PEDOT porous film displayed conductivity of about 195 S cm^{-1}. A DSSC device assembled from the as-prepared porous PEDOT film yielded a low PCE of 7.93% when compared to the Pt-based device with 8.7% PCE [3, 63]. Furthermore, using arrays of ZnO nanowires as templates, Trevisan et al. [64] electropolymerized nanotubes of PEDOT onto an FTO substrate. The as-prepared counter electrode displayed an efficiency comparable to that of classical Pt, and depending on the electrolyte used, it showed performance superior to Pt [3]. When compared to the bulky and unmodified counterparts, the PEDOT-nanotubes counter electrodes (CEs) demonstrated superior performance. A PCE of 8.3% was attained by the DSSC with PEDOT-nanotubes CE, comparable to that of the DSSC with Pt CE (8.5%) [3, 64]. The effect of morphology on the catalytic ability of the counter-electrode materials was made more apparent in the work conducted by Lee and coworkers [65]. By employing sodium dodecyl sulfate micelles as nanoreactors, PEDOT nanofibers (NFs) with dimensions of 10–50 nm and high conductivity of 83 S cm^{-1} were created. In their work, colloidal dispersion based on methanol was spin-coated to obtain the PEDOT-NFs. In comparison to bulk PEDOT (6.8%), the DSSC based on PEDOT-NF CE with low surface resistance and a highly porous surface attained a high PCE of 9.2% [65]. Moreover, it was more effective than classical Pt CEs (8.6%) in catalyzing the redox mediator [3, 65].

Similarly, mediators influence the performance of CE and the DSSC as a whole. The PEDOT-CE can display even greater performance when $Co^{3+/2+}$ is the redox couple for a DSSC device. For instance, PEDOT-CEs were fabricated via electro-oxidative polymerization by Tsao et al. [66]. The highest PCE (10.30%) was produced by the DSSC device with Y123-sensitized, cobalt-mediated, and PEDOT-based CE. This is because PEDOT significantly lowers the interfacial charge-transfer resistance and the mass transport limits, which leads to higher PCE values [3]. Likewise, Burschka et al. [67] also assembled a PEDOT CE –based DSSC with T_2 (dimer of 5-mercapto-1-methyltetrazoleion)/T− (5-mercapto-1-methyltetrazole ion) redox system.

The T-mediated DSSC with PEDOT CE yielded a PCE of 7.9, outperforming the cell with a Pt electrode in terms of their power conversion efficiencies.

2.2.2 Poly(3,4-propylenedioxythiophene)

Poly(3,4-propylenedioxythiophene) (PProDOT), due to its extremely high surface area and capacity to prevent the formation of any passivation layers at the electrode/electrolyte interface, outperforms Pt electrodes in DSSCs [3]. As of now, the data provided utilizing many other types of CEs is much lower than the PCE values of the DSSCs with PProDOT CEs [68-72]. For example, as compared to the Pt electrode (8.24%, 50 Ω cm^2), the cells using PProDOT CEs produced a 20% increase in PCE (9.9%) and a notable decrease in RCT (2.5 Ω cm^2) [71]. The PProDOT-based DSSCs with I-based and Co-based redox couples have PCE values of 9.25% and 10.08% respectively [3]. Moreover, the possibility of depositing PProDOT films on flexible substrates, makes them applicable in flexible DSSCs.

2.2.3 Polyaniline

Polyaniline (PANI), despite its discovery over a century ago, only received a lot of attention in the early 1980s [3]. This is because its desirable electrical conductivity only came to light in recent decades. In the last 5 decades, PANI is found to be one of the most researched conducting polymers within the family of conducting polymers and organic semiconductors [73-76]. PANI is particularly appealing due to its affordability, electrochromic properties, and redox activity [3]. The latter characteristic makes PANI appealing to biosensors, supercapacitors, and acid/base chemical vapor sensors [10]. The material is also promising for use in actuators, supercapacitors, and electrochromics due to the various colors, charges, and conformations of the various oxidation states. PANI is commonly employed in the manufacture of electromagnetic shielding, flexible electrodes, electrically conductive yarns, and antistatic coatings [77-81].

PANI is one of the most employed conducting polymers as a counter-electrode material due to its affordability, easy synthesis, high conductivity, excellent thermal and chemical stability, and intriguing redox characteristics [82, 83]. Generally, high surface area and high porosity are the common desirable features of PANI in their application as a CE material. PANI synthesized via electropolymerization has a well-connected structure resulting in superior performance [3].

Variations of PANI have been produced and utilized as CE materials for DSSCs over the years. The Wu group was the first to report the use of PANI as CE for DSSCs in 2008 [84]. They used an aqueous oxidative polymerization reaction using perchloride acid as a dopant in the presence of ammonium persulfate to create microporous PANI nanoparticles (NPs) with diameters of 100 nm. In their work, PANI demonstrated superior reductive electrocatalytic performance for the I_3^-/I^- redox process than the Pt electrode.

Furthermore, various morphologies, including nanofibers, nanobelts, and nanotubes of PANI have been fabricated [63-65]. For instance, an orientated PANI nanowire array was in situ fabricated to enhance the PANI films' electrocatalytic performance [85]. This way, any exposed polymer components will be efficient for the catalytic reduction of the oxidized species in the electrolyte because electron transportation through the PANI nanowires is rapid [3]. The PANI nanowire array outperforms the Pt electrode as well as the random PANI film in terms of electrocatalytic activity for the $Co^{3+/2+}$ redox process. The efficiency obtained using the random PANI film (5.97%) or the Pt cathode (6.78%) was much lower than that obtained utilizing the oriented PANI nanowire array as CE in a Co-based redox coupled DSSC, and with a FNE29 dye (8.24%) [3]. By utilizing electrospun vanadium pentoxide (V_2O_5) as a template and oxidant, followed by acid etching and in situ polymerization, Hou et al. [86] fabricated a PANI nanoribbon (NR) CE with serrated, flexible, and ultrathin nanostructures. The PANI-NR CE had significant catalytic activity due to its abundance of active sites and good contact performance, and the DSSC based on the PANI-NR CE attained a PCE (7.23%) comparable to that of classical Pt-based cell (7.42%).

In order to maximize the absorption efficiency of the incident light, PANI can be fabricated as transparent films that can be employed in bifacial solar cells [3]. In this regard, Tai and coworkers fabricated a very homogeneous and transparent PANI film via a simple in situ polymerization process, and they employed it as CE in DSSCs [87]. An active transparent bifacial DSSC was developed using the as-prepared electrode, and it exhibited efficiencies of 6.54 and 4.26% for front- and rear-side irradiation, respectively. At the same time, a dye-sensitized cell assembled under the same conditions with platinum as the CE showed an efficiency of 6.69%. In contrast to traditional Pt-based DSSCs, the bifacial DSSC's architecture encourages the use of light from both sides of the electrodes. Wu demonstrated that more dye molecules are activated as a

result of simultaneous front and backside solar irradiation, which improves the short-circuit density J_{SC} and the overall power conversion efficiency [88]. The 4-Aminothiophenol (4-ATP) modification of PANI resulted in an improvement of its photoelectric characteristics. In comparison to the DSSC irradiated from the front only, the bifacial DSSC with 4-ATP/PANI CE obtained an overall conversion efficiency of 8.35%, which is a 24.6% increase in efficiency [88].

The morphologies, electrochemical characteristics, and doping/de-doping processes of polymer films are greatly influenced by doping ions. Dopants such as TsO (Ts = tosyl), PSS, ClO_4, SO_4^{-2}, ClO_4^-, Cl^-, and BF_4^-, have been utilized in the design of CEs [68, 89-91]. The SO_4^{-2}–doped PANI film stood out in terms of its higher porosity, higher current for the reduction of triiodide, and lower charge-transfer resistance (1.3 Ω cm^2) in comparison to Pt CE, attaining a PCE of 5.6% [91]. Meanwhile, the PANI film that was doped with sodium dodecyl sulfate (SDS) showed an increased conductivity and catalytic reduction of triiodide exhibiting a PCE of 7.0%, similar to that of a Pt-based DSSC (7.4%) [92].

The solvent system in which the polymer-based CE is fabricated can also significantly influence the catalytic performance of the CE. Chiang and colleagues demonstrated that polymer films (PANI-SO_4–F or PEDOT–F) can be easily fabricated on a TCO by spin coating or casting from the relevant solutions at room temperature to give CE materials with desirable conductivity, good adhesion, excellent conductivity, and good electrochemical properties [93]. They employed Hexafluoro-isopropanol (HFIP), a nontoxic solvent, to produce PANI/HFIP and PEDOT/HFIP colloid solutions that are extremely concentrated and stable by simply dissolving the doped polymer powders in HFIP. The conversion efficiencies of the DSSCs based on PANI-SO_4-F and PEDOT-F CEs, with the combination of CYC-B11 sensitizer and triiodide/iodide electrolyte, were 8.8% and 9.0%, respectively, which is comparable to the classical Pt-based dye-sensitized cell of 8.9 % PCE.

PANI as a CE electrode material offers superior catalytic activities, high conductivity, straightforward synthesis, and inexpensive cost making it a good replacement for the expensive Pt electrode. However, PANI is relatively unstable, self-oxidizing, and its carcinogenic properties make PANI relatively less ideal as a CE material [94].

2.2.4 Polypyrrole

Polypyrrole (PPy) was first reported in 1963 by Weiss and his coworkers [95]. They explained how tetraiodopyrrole's pyrolysis led to the production of highly conductive materials. By polymerizing pyrrole, an organic polymer known as polypyrrole is created. Although PPy films are yellow, slight oxidation causes them to darken in the air. Depending on the degree of polymerization and film thickness, doped films can be either blue or black. They are amorphous and only exhibit marginal diffraction [3]. As there is some chain hopping and crosslinking, PPy is referred to as "quasi-one-dimensional" as opposed to one-dimensional. Both undoped and doped films of PPy are swellable but insoluble in solvents [96]. PPy possesses considerable thermal stability in elevated temperatures up to 150 ^{o}C [97, 98].

Although PPy is an insulator, its oxidized derivatives are excellent electrical conductors. The oxidation conditions and reagents used has a great influence on the conductivity of the material. PPy is commonly found useful in electronic devices and chemical sensors [99-101]. Ease of synthesis, good catalytic activity, low cost, high polymerization yield, and significant environmental stability are some of the desirable features that make PPy a suitable option for the replacement of Pt CE [98, 102-104].

In 2008, Wu et al. [102] reported the use of PPy as a CE material in DSSCs for the first time. But before that, PPy was employed as hole conductor in solid-state DSSCs [105, 106]. Wu and coworkers chemically polymerized PPy nanoparticles with the aid of an iodine initiator [102, 107]. The synthesized nanoparticles of PPy were deposited onto an FTO substrate and employed as a CE for DSSC. Structural characterization indicates that the as-prepared PPy film is porous, uniformly, and tightly coated on the FTO with particle diameter in the range of 40 to 60nm. Moreover, PPy CE displayed better electrocatalytic activity with lower charge transfer resistance when compared with Pt CE. The DSSC assembled with PPy CE exhibited a PCE of 7.66%, outperforming the DSSC device with expensive Pt CE (6.90% PCE).

In the synthesis carried out by Jeon and coworkers, they fabricated isolated spherical PPy nanoparticles with the aid of micelles, consisting of N, N, N-Trimethyl-1-tetradecanammonium bromide and capric alcohol nanoreactors, yielding nanoparticles with diameter and conductivity of approximately 85 nm and 10 S cm^{-1} respectively [98]. They achieved a significant reduction of

the surface resistivity of PPy film (624–387 Ω-2) by doping with concentrated hydrochloric acid gas for 1 minute. The PCEs of 6.83 and 5.28%, were attained by doped- and undoped-PPy CEs-based DSSCs respectively. Additionally, by adjusting the electrolyte composition, the cell efficiency of the cell based on PPy CE was raised to 7.73%. Furthermore, Pen et al. [103] successfully fabricated discrete PPy nanotubes via a relatively simple technique involving heating uniform pulp-like solutions at reduced temperatures, which could be utilized in flexible substrate-based DSSCs. It is worth noting that the conversion efficiency of the DSSCs based on these flexible PPy membranes is 5.27%, which is around 84% of the cell with a typical Pt/FTO CE (6.25%).

Hwang et al. [104] innovatively fabricated a CE based on PPy where they utilized sodium decylsulfonate (SDSn) as a template to create extremely thin PPy nanosheets via organic single-crystal surface-induced polymerization (OCSP). These ultrathin PPy nanosheets possess a morphology comparable to graphene sheets in terms of having higher surface area and active sites [3]. The ultrathin PPy nanosheets, deposited onto an FTO substrate as a CE for DSSCs, possess exceptional transparency of about 94%, which was attributed to its nanoscale thickness. Similar to the work done by Jeon and his coworkers [98], the conductivity of PPy was increased upon doping with HCl gas, and evidence provided by data from Tafel polarization and impedance confirms the improvement of catalytic activity of the HCl-doped CEs. A PCE of 6.8%, comparable to Pt-based DSSCs of 7.8% PCE, was achieved for the DSSC with HCl-enhanced ultrathin CEs, which is 19.3% higher than the un-doped PPy CE-based DSSC. Additionally, due to its high transmittance, room temperature processing, and two-dimensional structure, the ultrathin PPy nanosheet is appropriate for flexible devices.

Many studies and applications of PPy as CE materials in DSSCs have been conducted [98, 102-104, 108-114]. Because of its simple synthesis, superior air stability, affordability, and high polymerization yield, PPy is one of the many conducting polymers that is of particular interest for its application as counter-electrode material [115]. However, the application of PPy as CE materials for DSSCs is limited by its relatively low conductivity and high charge transfer resistance [4]. The dopant, morphology, and synthesis method employed greatly influence the catalytic performance of PPy as CEs in DSSCs [3].

Even though polycarbazole (PCbz) possesses good conductivity, to the best of our knowledge, there is no literature on PCbz as a counter-electrode material in DSSCs. This could be due to its poor stability when in contact with redox mediators in DSSCs. However, among most of the conducting polymers that have been employed as counter-electrode materials, PEDOT-based CEs display higher photovoltaic performance and have great prospects in replacing Pt as CE for DSSCs [3]. But generally, conducting polymers can have their features readily modified or tuned [3, 4]. Flexibility, optical transparency, ease of processability, and scalability for mass production are all characteristics of suitable conductive polymers as CE materials for DSSCs [3]. They are capable of acting as both substrates and catalysts. Consequently, there is great potential for replacing TCO and Pt as substrates and CEs respectively, and thus the plausibility of drastically reducing the cost of DSSCs by more than 50% [4].

2.3 Determinants influencing the catalytic ability of polymer-based counter electrodes

The electrical conductivity, catalytic activity, surface area, matching energy levels of components, electrochemical and mechanical stability, thickness, porosity, adhesion, particle size, and structure of the CEs materials all have an impact on how well they perform in a DSSC device [136-138]. Some important elements that have a significant impact on polymer CE performance are addressed in the section that follows.

2.3.1 Conductivity

The CE is crucial in facilitating the flow of electrons from the external circuit back to the redox mediators. Hence, for the majority of CEs, greater electronic conductivity is also greatly desired. Nevertheless, not all of these CE catalysts have higher electronic conductivity comparable to well-known CE materials such as carbon compounds, polymers, and early transition metal complexes (TMCs). As a result, polymers, graphene, carbon black, and carbon nanotubes (CNTs) are often used as components of hybrid CEs to enhance the conductivity of CE materials in DSSCs [116-135].

2.3.2 Electrocatalytic activity

The catalytic activity is a crucial element that determines how well CE catalysts operate in their function as a catalyst for the reduction of redox mediators in a DSSC. The availability of

additional catalytic sites, which results in increased catalytic activity for the reduction of the redox couple, makes it crucial for CE materials to have high specific surface areas [155]. This property accounts for the frequent usage of mesoporous polymers as CE catalysts in DSSCs [139-143]. Pt metal's exceptional catalytic activity and conductivity have also demonstrated that it makes a great catalyst. In theory, Pt-like catalytic activity might be produced by CE materials with an electronic structure resembling that of Pt metal [144-147]. For this reason, quite a wide range of transition metal complexes such as carbides, oxides, selenides, nitrides, sulfides, etc. have been evaluated as replacements for Pt CEs in DSSCs [140,148]. But most often than not, the physical and chemical properties of these Pt-substitute CE materials typically fail to live up to expectations. [140,141, 143, 149]. For this reason, polymer-based composite CEs are usually created to increase their catalytic activity by taking advantage of the synergistic effects of the various components of the composites.

2.3.3 Morphology

The photovoltaic (PV) properties of DSSCs are significantly influenced by the architecture of the CE materials, which plays a major role in how well CE catalysts work. Research points to the following: (1) the greatest PCE that has been observed for PPy CEs in various types of DSSCs is 7.73% for spherical PPy in iodine-mediated DSSCs with N719 dye [150]; (2) in iodine-mediated DSSCs with N719 dye, PEDOT nanotube arrays produce a PCE of 8.3%, while plain PEDOT films produce a lower PCE value of 7.9% [151]; (3) but in iodine-mediated DSSCs with N719 dye, PEDOT nanofibers produce a PCE of 9.2%; however, atomic force microscopy (AFM) analysis caused a rise in the surface roughness value of PEDOT nanofibers from 69.9 nm to 90.5 nm, which consequently reduced the PCE value from 9.2% to 8.3% [152]; and (4) in cobalt-mediated dye-sensitized cells with FNE29 dye, PANI nanowire arrays displayed an efficiency of 8.24%, whereas PANI films with random networks, obtained via drop-casting, displayed an efficiency of 5.97% -making the effect of the morphology on the catalytic ability of polymer-based CEs in DSSCs apparent [153]. Tantalum oxides, tungsten oxides, and niobium oxides are examples of inorganic compounds where their morphology and crystal structures as CE materials had a similar impact on their catalytic abilities in DSSCs [137,138, 154].

2.4.4 Stability

In DSSCs, both electrochemical stability and mechanical stability significantly impact the pragmatic application of CE materials. The electrochemical stability is often used to predict how the polymer-based CE materials will respond to redox couple electrolytes like I_3^-/I^-, T_2/T^-, and Co^{3+}/Co^{2+}—mostly whether there is any swelling or reaction [155]. To assess the electrochemical stability in catalyzing the reduction of common redox mediators in DSSC devices, employing typical CE materials, dark J-V tests on the assembled cells, successive cyclic voltammetry (CV) scans, and electrochemical impedance spectroscopy (EIS) tests on the symmetrical cells are usually carried out [140]. Although it is currently unclear how the CV and EIS curves of multi-cycle successive scans report on polymer CE stability in DSSCs, There are no unusual deviations from these curves, which suggests that these polymer-based CEs will be unreactive towards the electrolytes [155]. Much consideration, however, should be given to the interface adhesion between the CE films and the substrates in CV and EIS analysis [155]. Carbon materials as CEs, while promising substitutes for Pt-CEs, are currently limited in their industrial-scale application in DSSCs due to their mechanical stability and poor adhesion to the substrate [155]. As a result, the improved mechanical and electrochemical stability of polymer-based CEs with better catalytic activity and conductivity benefits the promotion of large-scale industrial applications of DSSCs [3,155].

2.3.5 Matching cell components

The utilization of optimized cell components and matching of energy levels of cell components are crucial for the enhanced performance of DSSCs. Thus, to maximize the performance of the polymer CE, the most suitable sensitizer and redox couples should be used [155]. The best PCEs for the combinations of N719 dye and the iodine-based mediator, Y123 dye and the cobalt-based mediator, and Z907 dye and the T-based mediator with PEDOT films as CEs in DSSCs are 8.0%, 10.3%, and 7.9% respectively, as discussed in section 2.1 [62, 67,68, 70]. Moreover, when using PProDOT films as CEs in DSSCs, N719 dye and the I-based mediator and Y123 dye and the Co-based mediator are the best pairings yielding PCEs of 9.25% and 10.08%, respectively [70, 71]. In addition, dye N719 has proven to be better suited than dye Z907 in enhancing the photovoltaic performance in iodine-mediated DSSCs with PPy CEs [155]. For PANI

CEs, the devices assembled with dye-FNE29 and Cobalt-based mediator as well as dye-N719 and the iodine-based mediator, display superior performance to the cells assembled with the dye-N3 and the I-based mediator combination in DSSCs [155]. On the other hand, the most suitable dye for bifacial transparent DSSCs is the dye-N3 due to its ability to enable better absorption of incident sunlight from both sides of the devices [155]. Most polymer-based CEs operate more efficiently with dye-N719 than with dyes Z907, -N3, and -Ru535 in iodine-mediated DSSCs [3, 70, 155].

2.4 Enhancing polymer-based counter electrodes

Small amounts of platinum metal are usually required in fabricating Pt-CEs. However, Pt is considered a critical raw material (CRM) and is a rare earth metal [3, 155]. In addition, Pt decomposes in the redox couple during the DSSC operation and most often than not, leads to the creation of new charge recombination sites limiting the PCE of the device [155]. Therefore, due to their desirable properties like less electrical resistance, low cost, and excellent electrocatalytic activity in oxygen reduction reactions (ORR), carbonaceous materials have been utilized as replacements for the expensive Pt metal [155]. Conducting polymers can be altered to create tunable micro- and nanostructures with desirable conductivity levels, making them excellent potential ORR candidates. At room temperature, a variety of wet procedures can be used to deposit polymer-based CE catalysts. It is also advantageous that these catalysts could be deposited on flexible substrates. It is possible to fabricate polymer-based CE catalysts with large surface areas via straightforward procedures such as electrochemical deposition, slot dye coating, dip coating, thread coating, or printing methods. Research shows that polymer-based CEs may function better than Pt electrodes [1-5, 10, 53, 56, 57]. This is mostly because of their greater surface area, which encourages improved electro-catalytic properties. Finding novel methods to create CPs with high conductivities and tunable morphologies is therefore crucial to enhancing the catalytic ability of polymer-based CEs.

CPs can be doped to adjust their physicochemical parameters so as to achieve high conductivity that can compete with metal-based electrocatalysts [61, 62, 84]. Due to their high surface areas and high conductivity, polymers with nanoporous structures are capable of producing more electrocatalytic active sites, while facile electron mobility is promoted by their high conductivity [3,93, 155].

Another way to enhance polymer CEs is via the rational modification of their structures [3, 63-65]. For instance, one-dimensional structures of rationally engineered polymers can significantly enhance their conductivity, but unfortunately, progress in this kind of improvement of CEs is severely hampered when it comes to large-scale production, and utilizing templates also restrict their production [155].

The synthesis of novel polymer-based CEs that can replace Pt CEs will be considerably improved via uniform, conformal, and controlled thickness [85, 86, 87]. However, a balance must be struck in this trade-off. For instance, polymers with less thickness will result in the lower active surface area while offering higher conductivity [155]. Conducting polymers can be modified for their electro-optical activity, opening up the possibility of creating solar windows or building integrated photovoltaic systems with controllable electrochromic properties [155]. Generally, stability, high surface areas, electrochemical reversibility, and low band gap are desired features mostly required of polymer-based CEs.

2.5 Counter-electrode characterization

In order to fabricate new materials and enhance the photovoltaic performance of DSSCs, several characterization techniques have been created to comprehend the morphology of DSSC components and understand the relative reaction process mechanisms, such as charge creation, charge transfer, and charge recombination [172-174]. Considered the most effective tools for structural characterization, analyzing the process pathways, evaluating component interactions, and assessing DSSC performance have been microscopy, spectroscopy, and electrochemical techniques [175-177]. Some of these include Scanning electron microscopy, energy dispersive X-ray spectroscopy, transmission electron microscopy, X-Ray diffraction, X-ray photoelectron spectroscopy for structural characterization, and current–voltage characterization, cyclic voltammetry, and electrochemical impedance spectroscopy for electrochemical analysis.

2.4.1 Structural characterization

2.4.1.1 Electron microscopy

Scanning electron microscopy (SEM) is a technique for examining the surface morphology of nanostructures by measuring the scattering of highly energetic-electron beams from the surfaces

of nanomaterials [157]. One of the traditional and accepted approaches for microscopy studies of nanostructure film morphologies of DSSC components, such as counter electrodes, is SEM [158, 158]. The thickness of counter-electrode films, which can be determined via cross-sectional SEM, has a significant influence on their catalytic performance [159]. By utilizing the SEM technique, Ellis et al. [160] for instance, evaluated potential variations in the electro-activity of the PEDOT counter electrodes with varying porosities and thickness in the device achieved via different electrochemical deposition techniques.

Apart from SEM, energy dispersive X-ray spectroscopy (EDX) can also be used to study the thickness of the counter electrode film as well as the film's constituent elements-elemental analysis. EDS typically has a resolution of several hundred nanometers and is very useful for elemental mapping composite materials [161-163].

Furthermore, transmission electron microscopy (TEM) is another electron microscopic technique that is commonly used for the structural characterization of DSSCs components, especially the CEs. TEM, which usually provides more in-depth information about a material, usually employs higher energy electron beams than SEM, thus allowing for the analysis of features as small as a few nanometers. Moreover, even finer details of film crystalline planes as small as a few Angstroms can be observed using high-resolution transmission electron microscopy (HRTEM). In addition, atomic force microscopy (AFM), although not as popular as SEM or TEM is capable of examining the surface morphology of CEs material of DSSCs [164-167].

2.4.1.2 X-Ray diffraction (XRD)

XRD is a very useful technique for investigating the crystallinity of nanomaterials. In a typical XRD, a short wavelength X-ray photon is scattered by an electronic cloud of highly organized positive ion centers within the material, causing a diffraction pattern to appear as a result [157]. With XRD, it is also possible to identify the regularity and order of the ions that are creating a lattice in the sample [168]. Novel counter electrode materials are frequently investigated to analyze their crystallinities via XRD [158, 169, 170].

2.4.1.3 X-ray photoelectron spectroscopy (XPS)

The photoelectric effect is utilized in XPS where electrons can be ejected from a material by illuminating the material with X-rays to determine its binding energy and the work function. Each element has unique binding energies for energy levels from atom-like orbitals, XPS can therefore reveal information about the elemental makeup of surface atoms. Sensitive to chemical changes or the electrical environment of particular atoms, XPS can reveal a material's chemical state. By using XPS, different DSC components can be investigated. More understanding of the energy levels involved in the electron transfer mechanisms in DSSCs can be provided by the measurement of the valence energy levels using XPS [157]. The work conducted by Shi and coworkers, where novel counter-electrode material was evaluated, is an example of how XPS may be used to study the atomic composition of newly introduced DSC components [171].

2.4.2 Photovoltaic measurements

The correlation between the output current and voltage of the solar cell under typical full spectrum illumination is represented by the current-voltage (I-V) characteristic curve, which is used to calculate the photovoltaic parameters of the cell. The intercepts of a typical I-V curve in the horizontal and vertical axes are respectively, the open circuit voltage (V_{OC}) and short circuit current (I_{SC}) or short circuit current density (J_{SC}) as depicted **in Figure 2**. J_{SC} denotes the cell's short-circuit current density at zero voltage, which represents the cell's maximum capacity for photocurrent output, and V_{OC} for the cell's open-circuit voltage at zero current, which represents the cell's maximum capacity for photovoltage output. The rectangular area of the meeting point of the photocurrent (I_{mp}) and photovoltage (V_{mp}) on the curve indicates the device's real maximum output power (P_{max}). The fill factor (FF), which has values ranging from 0 to 1, is the ratio of P_{max} to the product of V_{OC} and J_{SC} [3, 157].

The overall solar power conversion efficiency (PCE) of the DSSC is calculated as the ratio of the product of J_{SC}, V_{OC}, and FF to the power density of the incident light (P_{in}).

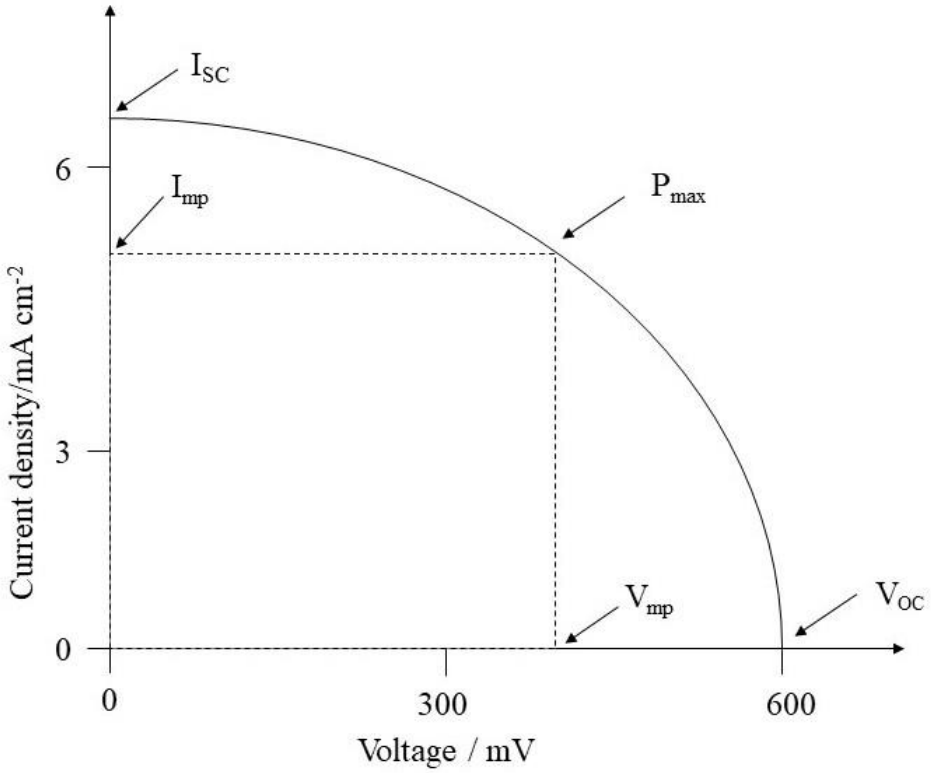

Figure 2. I-V curve for photovoltaic measurements of DSSCs.

2.4.3 Electrochemical techniques

2.4.3.1 Cyclic voltammetry (CV)

Electrochemical techniques can be used to characterize all the various constituents of the DSSC. Electrochemical techniques provide crucial knowledge on the energy levels of the constituents, and the redox and kinetics of electrochemical processes. For analyzing counter electrodes, CV is a crucial technique. A three-electrode classical system, consisting of a working electrode, a reference electrode, and a counter electrode is frequently employed to perform CV analysis. While closely keeping tabs on the current, the potential is swept at a consistent pace and then reversed at a specific point during a CV scan. Whereas the current is measured between the working electrode and the counter electrode, the potential is measured between the working

electrode and the reference electrode to obtain a plot of current (I) against potential (E). The formal redox potential, interface charge transfer rates, and the diffusion coefficient can all be calculated by scanning the voltage and observing the current in forward and backward scans [157,178]. Only capacitive current flows when the scan is initiated at a potential well positive of zero potential; once the decrease starts, faradaic current starts to flow. The current increases as the electrode potential decreases until the surface concentration of the electroactive species approaches zero, at which point it peaks and subsequently decreases as a result of the depletion effect resulting in the a typical peaked current–potential curve.

Counter electrode characterization can also be done using CV. By measuring the CV of the counter electrode in the presence of a redox couple, one can study the electrocatalytic properties and determine the effective surface area of the counter electrode via using peak current separations and magnitudes or exchange current density analysis of symmetrical cells in traditional Tafel plots. A counter electrode with improved electrocatalytic activity will have a low peak separation and larger peak currents. The counter electrode may also have a bigger surface area or a higher charge transfer rate as a result. For the best possible device performance, the measured electron transfer rates and energy levels in the CV are critical [3, 157].

2.4.3.2 Electrochemical impedance spectroscopy (EIS)

EIS is an extremely effective technique for analyzing the electrocatalytic activity of counter electrodes in DSSCs as well as the kinetics of charge transport and electron-hole recombination [180-182]. In theory, the sinusoidal current response is measured as a function of modulation frequency by perturbing the applied potential with a very small sine wave modulation. The applied perturbation and the measured response are used to calculate the impedance. The frequency domain voltage to current ratio is known as the impedance, which is a complex number [157]. Electrochemical parameters such as series resistance (R_S), charge transfer resistance (R_{CT}), diffusion resistance (Z_W), and constant phase element (CPE) can be obtained by fitting the measured data to the appropriate circuit utilizing a software, enabling for the assessment of the system's electrochemical properties [183]. Because each dielectric mechanism in an electrochemical system has a unique characteristic frequency, the EIS method can be used to analyze every electrochemical impedance and process in the system. A Nyquist plot or a Bode plot is widely used to visualize EIS data. A complete Nyquist plot for DSSCs typically consists

of three semicircles as depicted in **Figure 3**. The series resistance (R_S) is the starting point, which primarily accounts for resistance in the conductive substrate, connecting wires, etc. The R_{CT_1} at the CE/electrolyte interface is indicated by the first semicircle, while the R_{CT_2} at the anode/dye/electrolyte interface is indicated by the second semicircle. The Z_W is represented by the third semicircle, which is at low frequency and mostly not shown due to the close proximity of the two electrodes and the electrolyte's low viscosity [157].

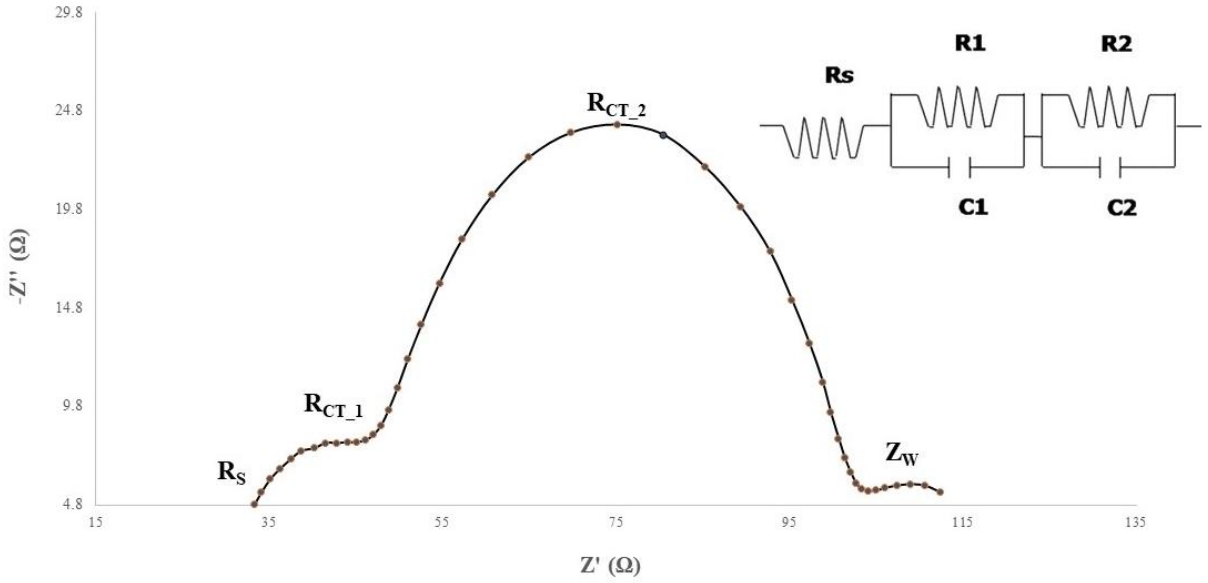

Figure 3. Classic Nyquist plot for liquid electrolyte based DSSCs

Most of the characterization techniques briefly highlighted in this thesis are also used to characterize other components of the DSSC. There are also other important methods that provide relevant information about the CE of a DSSC. However, the most fundamental ones are discussed in this work and can be sufficiently used to characterize counter electrodes of DSSCs.

3 Experimental

3.1 Materials

The materials utilized in this study were acquired from commercial sources. Chemical reagents, fluorine-doped tin oxide (FTO) coated glass slides (2.2 mm thick, surface resistivity about 7 Ω^{-2}), titanium IV isopropoxide, TiO_2 reflector paste (Greatcell Solar WER2-O, 150-250 nm), N719 dye (CAS Number: 207347-46-4), hexachloroplatinic acid-based Pt paste (Greatcell Solar PT1) were purchased from Sigma-Aldrich. The MPN-based iodide/triiodide redox electrolyte (DN-OD03) and transparent TiO_2 paste (DN-EP03, 18–20 nm) were acquired from Dyenamo (Sweden). NMR analysis (^{1}H NMR) was performed using JNM-ECA 500 MHz (Nazarbayev University).

3.2 Characterization and Measurement

The morphologies of the PEDOT and PEDOT:RCbz copolymer counter electrodes were observed with Scanning Electron Microscope JEOL JSM-IT200(LA) and Scanning Electron Microscope ZEISS Crossbeam 540 (Nazarbayev University). Cyclic voltammetry measurements were used to assess the electrochemical characteristics of CEs. CV was conducted using PalmSens4 Potentiostat / Galvanostat (PalmSens BV) with a three-electrode system in an acetonitrile solution containing 10 mM LiI, 1 mM I_2, and 0.1 M $LiClO_4$ at various scanning rates. Platinum (Pt) wire served as a counter electrode, silver-silver chloride (Ag/AgCl; in 3 M NaCl (aq) solution) served as a reference electrode, and as-prepared electrocatalyst covered FTO glass substrate served as the working electrode (WE) for electrochemical investigations. The photovoltaic measurements were performed using the Dyenamo Toolbox (DN-AE01).

3.3 Experimental procedures

3.2.1 Synthesis of N-alkyl carbazole derivatives

N-hexyl carbazole (Cbz-C6) synthesis was carried out according to ref. [184] with some modifications. Stirring for 30 minutes, 8.0 g of NaOH was dissolved in a dried 250 ml round bottom flask containing 60 ml of DMSO. Then 4.0 g of carbazole (24 mmol) was added, followed

by dropwise addition of 5.6 mL hexylbromide (39.98mmol). The product was isolated via filtration after cold water was added to the reaction, and washed three times with 50 mL of water before being dried over sodium sulfate and concentrated. The pure product was then obtained as crystals by column chromatography with 9:1 n-Hexane-ethyl acetate eluent system followed by drying under reduced pressure (5.7g, 94 % yield). ^{1}H NMR (Acetone-d_6, 500 MHz) δ 8.17 (d, J = 7.8 Hz, 2H), 7.60 (d, J = 8.1 Hz, 2H), 7.50 (t, J = 8.1 Hz, 2H), 7.24 (t, J = 7.8 Hz, 2H) 4.47 (t, J = 7.2 Hz, 2H), 1.94 (p, J = 7.5 Hz, 2H), 1.45 (m, 6H), 0.89 (t, J = 6.9 Hz, 3H).

This procedure was repeated for the synthesis of N-butyl carbazole (Cbz-C4, 87.7% yield).

Cbz-C4 ^{1}H NMR (Acetone-d_6, 500 MHz): δ 8.09 (d, J = 12.5 Hz, 2H), 7.60 (d, J = 8.1 Hz, 2H), 7.50 (t, J = 8.1 Hz, 2H), 7.24 (t, J = 7.8 Hz, 2H) 4.38 (t, J = 12.0 Hz, 2H), 1.89–1.79 (m, 2H), 1.43–1.35 (m, 2H), 0.93 (t, J = 12 Hz, 3H).

N-octyl carbazole was synthesized according to the procedure reported in reference with little modification [187]. Carbazole (1.67 g), bromooctane (2.88 g), and NaOH (1 mol, 4.00 g) were mixed in a flask containing 30 mL DMF. The mixture was kept stirring at room temperature for about 3 hours. After completion of the reaction (monitored by TLC), the mixture was neutralized with (10% dil. HCl) and the product was extracted with chloroform (15 mL 5 times). The combined organic extract was washed several times with distilled water and separated. After extraction, the organic extract was mixed with anhydrous sodium sulfate and stirred at RT for one hour to ensure complete dryness. Thereafter, the extract was filtered off, purified via column chromatography in hexane/Ethyl acetate solvent ration of 10:1, and the eluent was removed under vacuum till dryness to give 1.72 g(61.0 %) of compound as a yellow oil.

Cbz-C8 ^{1}H NMR (Acetone-d_6, 500 MHz): δ 8.1 (d, J = 12.5 Hz, 2H), 7.50 (d, J = 8.1 Hz, 2H), 7.40 (t, J = 8.1 Hz, 2H), 7.24 (t, J = 7.8 Hz, 2H) 4.4 (t, J = 12.0 Hz, 2H), 1.85–1.79 (m, 2H), 1.45–1.25 (m, 2H), 0.88 (t, J = 12 Hz, 3H).

3.2.2 Electrodeposition of polymer-based counter electrodes

Prior to the fabrication process, FTO substrates with dimensions of 1.5 cm ×2.0 cm were thoroughly washed in soapy water for 30 minutes, rinsed in deionized water, and washed in ethanol via sonication for 30 minutes. The FTO slides were then dried in the oven for at least two hours for at 70 ^{o}C. The copolymerization process was carried out according to the work done by

Akbayrak and coworkers [186] with some modifications. Monomers: EDOT, Cbz-C4, Cbz-C6, and Cbz-C8 were dissolved in DCM separately to prepare 10 mM stock solutions of each monomer. Then the monomer solutions were mixed in the ratio of 9.5:0.5, 9:1, and 6:4 (EDOT:Cbz-C4, EDOT:Cbz-C6, and EDOT:Cbz-C8; v:v) in separate vials. Carbazole derivatives-EDOT copolymers were electrodeposited onto the FTO substrates by potential cycling between −0.8 and +1.5 V vs. Ag/AgCl for 5 minutes in DCM-tetrabutylammonium hexafluorophosphate (TBU_4PF_6) electrolytic medium. PEDOT-based counter electrode was also fabricated under the same conditions for comparison.

3.2.3 Fabrication of dye-sensitized solar cell

The fabricating method for the dye solar cell was adopted from reference [185].Clean and dry FTO slides were submerged in a 50 mM titanium IV isopropoxide solution in HCl for 30 minutes. The slides were then sintered at 500 C for 30 minutes in order to deposit a compact TiO_2 coating. After applying transparent TiO_2 paste over the compact layer, the film was given a one-hour air drying period before being subjected to a series of stepwise sintering temperatures of 125 C, 325 C, 425 C, and 500 C. Then, a scattering layer of TiO paste was applied to the transparent TiO_2, dried for one hour in the air, and then sintered at temperatures of 125 ^oC, 325 ^oC, 425 ^oC, and 500 ^oC. The electrodes were placed into a 0.25 mM N719 dye solution in an acetonitrile:tert-butanol (1:1) solution after they were cooled to temperatures between 70 ^oC and 80 ^oC. The excess detached dye molecules were washed off the surface of the as-prepared TiO_2 electrodes with ethanol before drying to yield photoanodes. The DSSC was then assemble by dropping Iodide/triiodide redox electrolyte over the as-prepared TiO_2 photoanode, and a double-sided sticker was used to bind the EDOT and Cbz derivative copolymerized counter electrodes to produce four DSSCs for each poly(EDOT-Co-RCbz) sample. Four Pt counter electrodes as control devices were fabricated as well, by applying Pt paste on FTO substrates that were well cleaned and dried, and then sintered at 500 C for 30 minutes.

4 Results and Discussion

4.1. Material characterization

The 3 carbazole derivatives, (Cbz-C4, Cbz-C6, and Cbz-C8) were synthesized from simple 9H carbazole. The synthetic method employed gave 87.7%, 94%, and 12% yields for Cbz-C4, Cbz-C6, and Cbz-C8 respectively, suggesting that this synthetic is not very suitable for the Cbz-C8 derivative which gave a very low yeild. Unlike the synthesis of Cbz-C4 and Cbz-C6 which yielded solid products, synthesis of Cbz-C8 gave a liquefied product (oil) after drying under reduced pressure. The structures of the 3 carbazole derivatives were confirmed by ^{1}HNMR analysis (**Figure 4, 5, and 6**). The absence of an N-H chemical shift, and the presence of C-H alky shifts observed between 5ppm to 0.8ppm indicates a successful alkylation at N-position of the carbazole substrate. The counter electrodes were fabricated by anodic electropolymerization in a classical three electrode system consisting of a silver/ silver chloride reference electrode, platinum counter electrode, and pre-cleaned FTO glass slide as working electrode. The morphologies of the electrodeposited thin films counter electrodes (PEDOT and PEDOT:RCbz copolymers) were analyzed with SEM. The photographs and SEM images of the as-prepared films are shown in **Figure 7**. It can be observed that the thin film of PEDOT changes color from blue to dark blue upon copolymerization with carbazole derivatives. The SEM images also show a sponge-like structure of the PEDOT and PEDOT-RCbz films indicating that they are porous, which we believe will enhance the reduction of the triiodide redox mediator. The film's interface with the FTO is made stronger by the porous structure, which also encourages iodide/triiodide electrolyte permeability and facilitates faster charge transfer. Furthermore, the copolymerized films are more uniformly distributed than the PEDOT film, indicating that copolymerizing PEDOT with the carbazole derivatives favors uniform depositions.

The power conversion efficiency of DSSCs and incident light harvest are both significantly influenced by CE transmittance [3,157]. The transmittances of the four types of CEs are compared in **Figure 8**. The PEDOT-Cbz-C6 CE has the lowest transmittance which may be the deeper shade of black color forming upon copolymerization. This may have prevented light from passing through thus lowering the scattering of incidence light which is beneficial to the overall performance of the cell. Illumination from the rear however will be limited since the counter

electrode has low transmittance. PEDOT CE exhibits higher transmittance in the 300-800 nm wavelength range, which will possess a greater rear-illumination but higher light scattering.

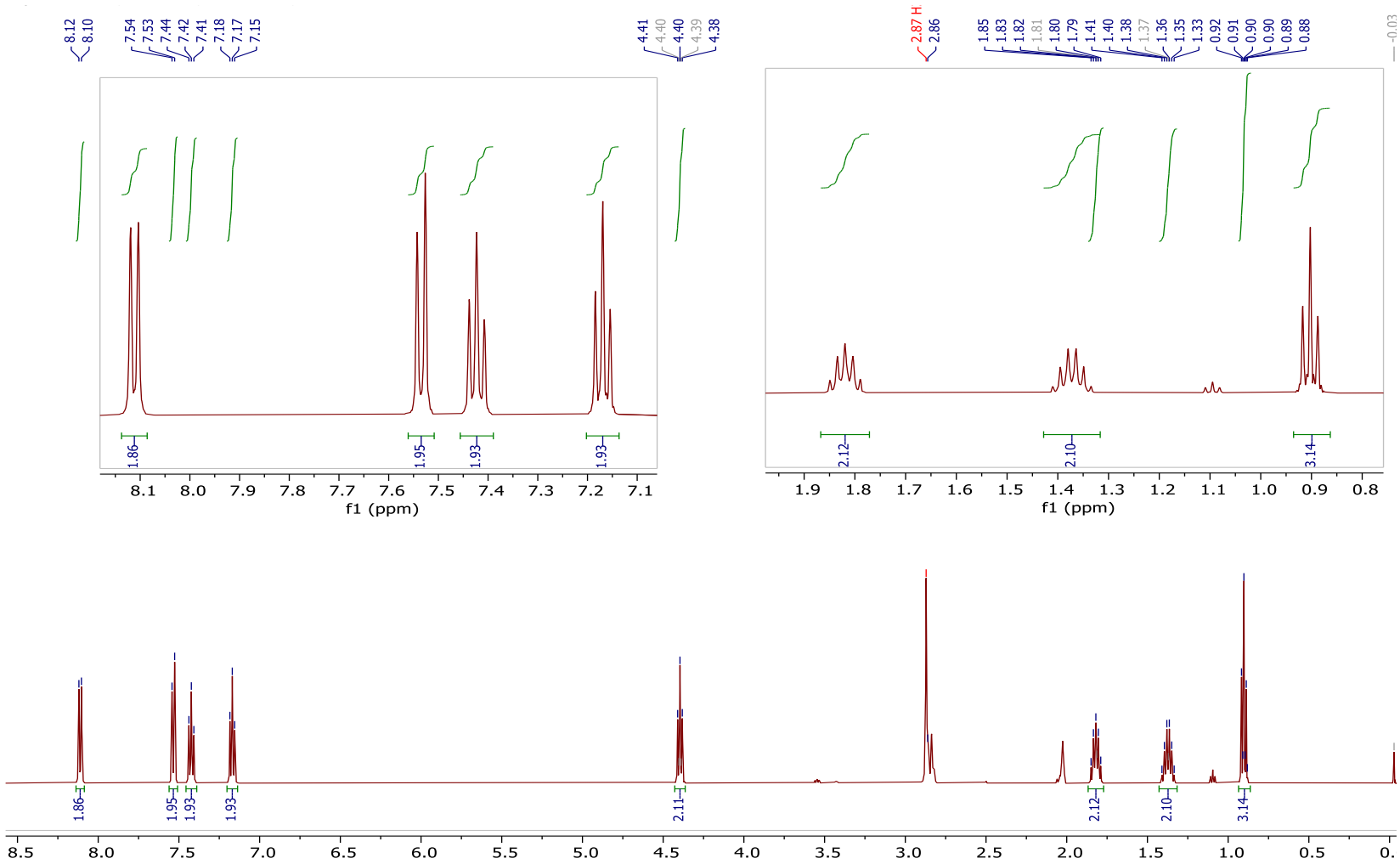

Figure 4. ^{1}H NMR of Cbz-C4

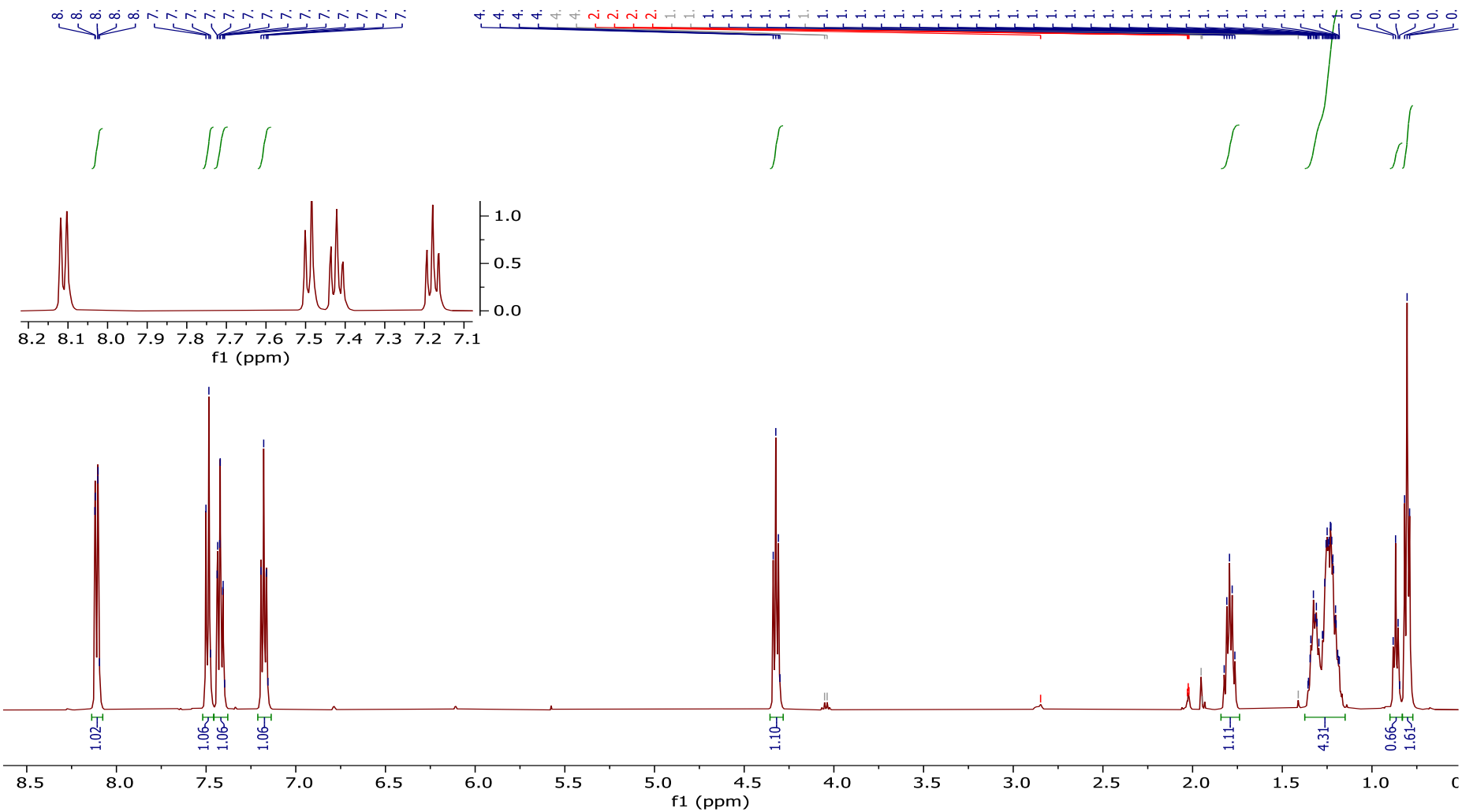

Figure 5. ^{1}H NMR of Cbz-C6

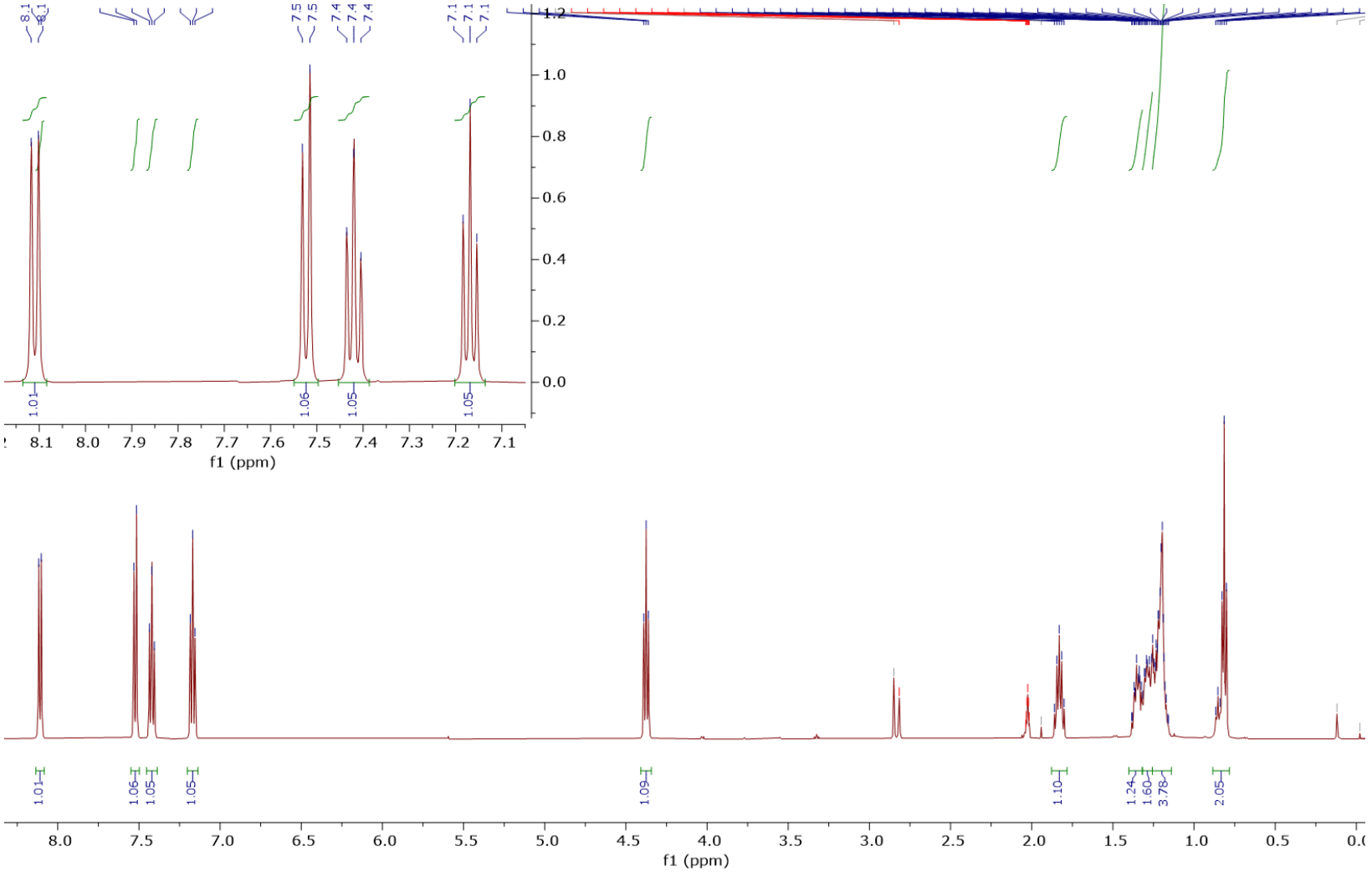

Figure 6. ^{1}H NMR of Cbz-C8

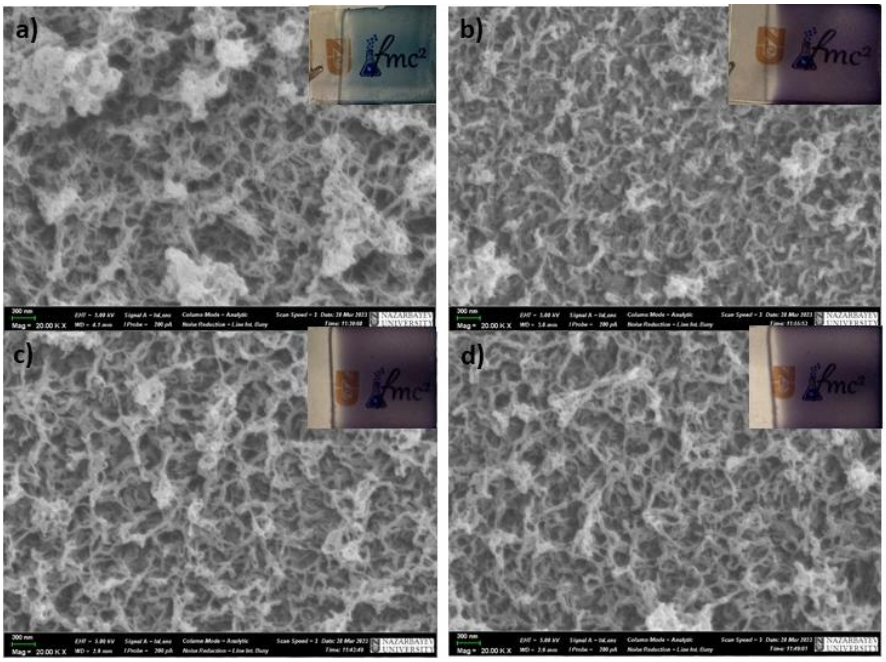

Figure 7. SEM images and photos of a)PEDOT, b)PEDOT-Cbz-C4, c) PEDOT-Cbz-C6, and d)PEDOT-Cbz-C8 counter electrodes (top view)

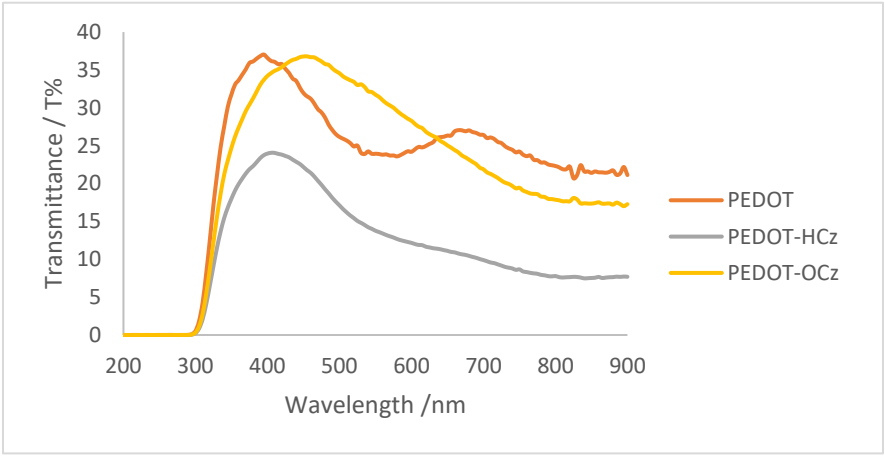

Figure 8. UV-vis transmittance spectra of PEDOT, PEDOT-Cbz-C6, and PEDOT-Cbz-C8 counter electrodes.

The electrochemical behaviors of CEs toward the I^-_3/I^- redox reaction were studied using cyclic voltammetry to better understand the catalytic mechanism of as-fabricated CEs. The CV curves of the PEDOT, PEDOT-Cbz-C4, PEDOT-Cbz-C6, PEDOT-Cbz-C8, and Pt electrodes in the acetonitrile solution with LiClO4 as the supporting electrolyte and LiI and I_2 as the redox couple are shown in **Figure 9**. Evidently, the five CEs each showed two usual pairs of oxidation/reduction peaks. It is widely known that the redox pair at comparatively positive potentials corresponds to redox reaction 1, while the redox pair at significantly more negative potentials corresponds to redox reaction [3, 68, 157].

$$3I + 2e \longrightarrow 2I_3^- \text{ ---------- (1)}$$

$$I_3^- + 2e \longrightarrow 3I^- \text{---------- (2)}$$

In evaluating the catalytic ability of a counter electrode in DSSCs, the reduction peak of the second reaction (2) is the main focus of CV analysis because the produced I_3^- ions are reduced to I^- at the CE/electrolyte interface. Peak current density and cathodic peak potential for the PEDOT-based electrode are remarkably greater as compared to the Pt electrode, suggesting that the I_3^- /I redox pair can be better electrocatalyzed by the PEDOT electrode. Similarly, the electrocatalytic ability of the PEDOT CE is increased when copolymerized with the carbazole derivatives, with intensities of the redox peaks increasing with increasing N-alkyl chain on the carbazole from the PEDOT-Cbz-C4 to PEDOT-Cbz-C8. This may imply an increasing reduction rate at the electrodes with increasing N-alkyl chain length. The PCE values measured and recorded in **Table 1** also corresponds to this observed trend. In addition, **Figure 10** shows CVs of the fabricated counter electrodes measured at various scan rates to test their stability in the iodine/triiodide redox mediator.

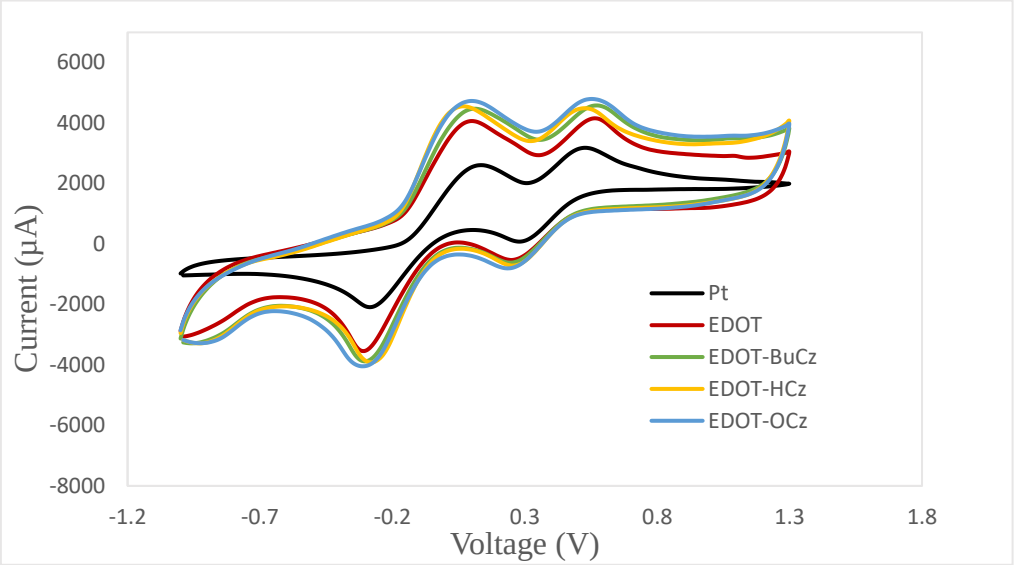

Figure 9. Cyclic voltammograms of Pt and polymer counter electrodes

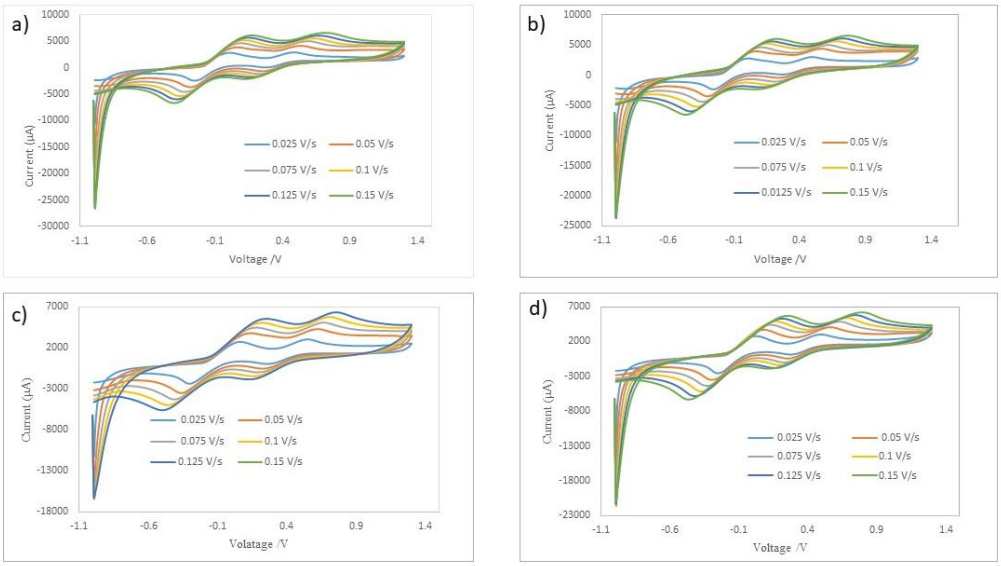

Figure 10. Cyclic voltammograms at different scanning rates for a)PEDOT, b)PEDOT-Cbz-C4, c) PEDOT-Cbz-C6 and d)PEDOT-Cbz-C8 counter electrodes

4.2 Device characterization

Measurements of the photovoltaic and electrochemical performance of the polymer electrode in dye-sensitized solar cells were conducted. DSSC photoelectric parameters such as open circuit voltage (V_{OC}), short circuit photocurrent density (J_{SC}), fill factor (FF), and total power conversion efficiency are given in **Table 1** in addition to the series resistance and charge transfer resistances (R_S, R'_{CT}, R_{TiO2}). The I-V curves and Nyquist plots are also illustrated in **Figure 11**. The photoelectric characteristics of the DSSC with polymer electrodes (PEDOT~7.9 ± 0.04%, PEDOT-Cbz-C4~8.0 ± 0.06%, PEDOT-Cbz-C6~8.5 ± 0.04%, PEDOT-Cbz-C8 ~8.9 ± 0.09%) are higher than those of the DSSC with Pt electrode (~7.6 ± 0.2%). Some factors could be attributed to the improvement of photoelectric performances of DSSC with the polymer counter electrodes. The morphology of the CE electrode, as discussed in the second Chapter of this thesis, plays a significant role in an electrocatalyst's ability to reduce the redox mediator. In this case, the counter electrodes coated with porous sponge-like structures of PEDOT films and PEDOT-co-carbazole derivatives possess significant active surface area on the electrode and can exhibit exceptional stability by trapping liquid electrolyte in the microporomerics. An increase in the counter electrode's surface area [6,8], can lead to a notable increase in the iodine/triiodide redox reaction rate occurring at electrode interface, thereby enhancing the DSSCs' photoelectric performance. Moreover, the polymer-based counter electrodes have smaller charge transfer resistance at the CE/electrolyte interface. The R'_{CT} value decreases from Pt (18.21 Ω) device to PEDOT-Cbz-C8 (14.00 Ω) device as shown in Table 1. Electron transport and the improvement of photocurrent density are both influenced by the least resistance (R'_{CT}) at the electrode/electrolyte interface for the iodine/triiodide redox reaction. This can therefore lead to the accumulation of iodine ions closer to the dye thereby accelerating the dye regeneration process [1]. The higher current density observed for the copolymer CEs can also be attributed to this.

Table 1

EIS and Photoelectric parameters of Pt and the polymer-CE DSSCs (average of three cells)

DSSC	Eff (%)	Voc (V)	J_{SC} (mA/cm^2)	FF	R_S (Ω)	R'_{CT} (Ω)	R_{TiO2} (Ω)
Pt	7.57 ± 0.2	0.74 ± 0.02	15.95 ± 0.4	0.64 ± 0.03	31.00 ± 0.2	18.21 ± 0.1	54.99 ± 0.4
PEDOT	7.90 ± 0.04	0.74 ± 0.007	16.02 ± 0.16	0.68 ± 0.009	29.41 ± 0.3	17.89 ± 0.3	40.54 ± 0.4
PEDOT-Cbz-C4	8.00 ± 0.06	0.72 ± 0.01	16.24 ± 0.15	0.69 ± 0.008	26.38 ± 0.2	17.55 ± 0.3	41.75 ± 0.3
PEDOT-Cbz-C6	8.52 ± 0.04	0.74 ± 0.01	16.31 ± 0.03	0.70 ± 0.003	24.00 ± 0.3	16.71 ± 0.1	42.23 ± 0.3
PEDOT-Cbz-C8	8.88 ± 0.09	0.76 ± 0.01	16.65 ± 0.27	0.71 ± 0.07	21.00 ± 0.2	14.00 ± 0.1	46.79 ± 0.4

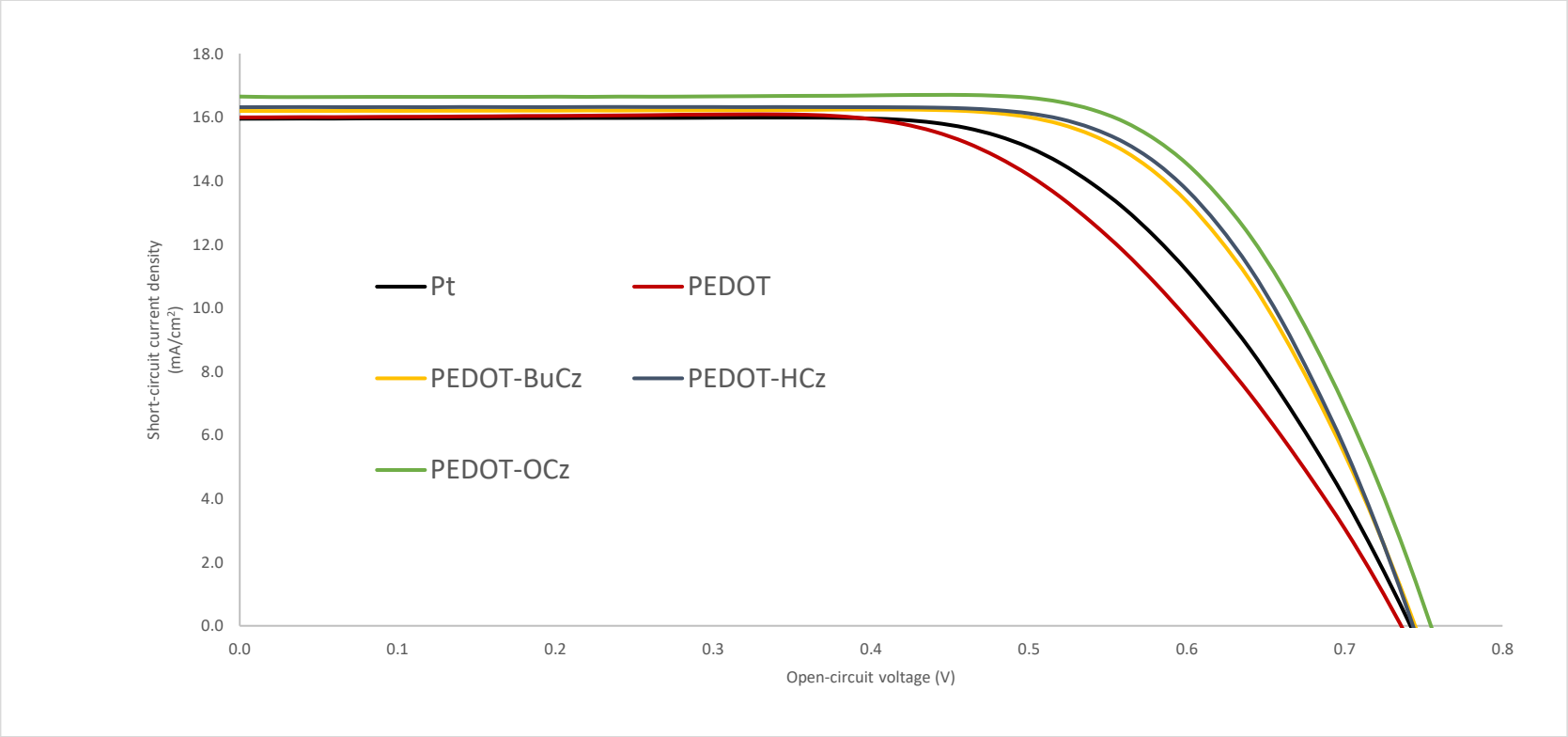

Figure 11. I-V curves of DSSCs with PEDOT, PEDOT- Cbz-C4, PEDOT-Cbz-C6, PEDOT-Cbz-C8 and Pt counter electrodes.

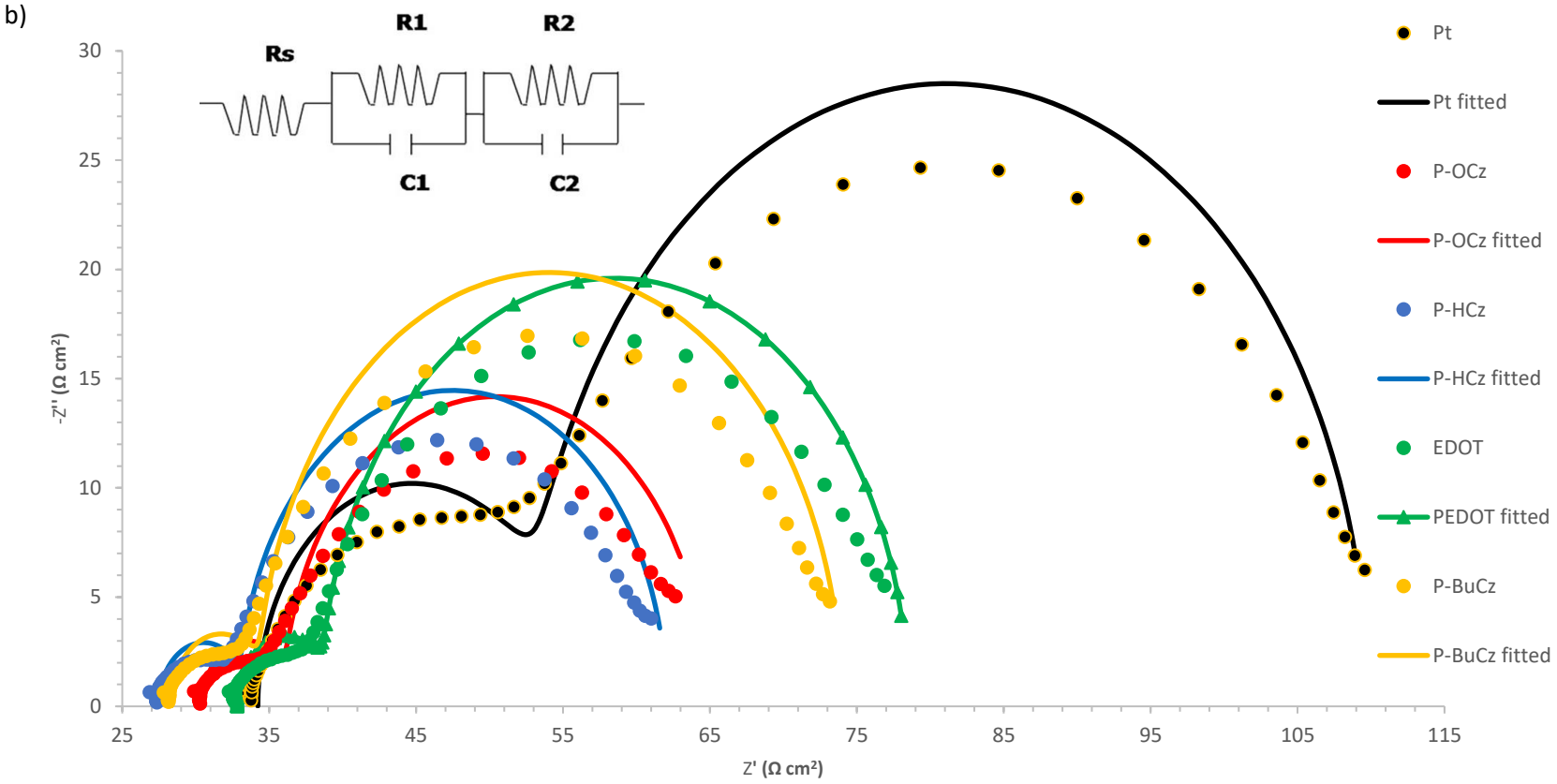

Figure 12. Nyquist plots of DSSCs with PEDOT, PEDOT- Cbz-C4, PEDOT-Cbz-C6, PEDOT-Cbz-C8 and Pt counter electrodes.

5 Conclusion and Future Direction

In summary, our research group, fmc^2 has successfully fabricated a relatively affordable counter electrode based on copolymers of PEDOT and three carbazole derivatives as a substitute for the traditional platinum electrode for catalyzing the iodine/triiodide redox reaction in dye-sensitized solar cells. A very simple and cheap electrochemical deposition method was employed in the fabrication processes. Scanning electron microscopic investigations indicated that the fabricated polymer counter electrodes attained a porous sponge-like morphology, and the films were uniformly coated onto the FTO glass substrate. DSSC based on PEDOT CE (PCE=7.9%) attained a higher efficiency than that of the DSSC based on Pt counter electrode (PCE ~7.6%) under the same conditions. Interestingly, the efficiency of PEDOT is enhanced when EDOT was copolymerized with the carbazole derivatives. The highest efficiency is produced by the copolymer based CE with the longest N-alky chain (PEDOT-Cbz-C8) on the carbazole, giving a PCE value as high as 8.8% and the highest density current value of 16.65 mA/cm^2. In this regard, our future work includes copolymerizing longer N-alkyl chains-based carbazole derivatives with PEDOT and to investigate their photovoltaic and electrochemical properties in an attempt to optimize the overall catalytic performance and stability of these CEs. This work demonstrates that PEDOT-Cbz-C8 CE is a promising replacement for platinum as a result of its superior PCE, photoelectric characteristics, simple fabrication process, and affordability.

References

[1] Tyagi, H.; Chakraborty, P. R.; Powar, S.; Agarwal, A. K. *Solar Energy: Systems, Challenges, and Opportunities*; Springer Singapore: Singapore, 2020.

[2] Ahmed, U.; Alizadeh, M.; Rahim, N. A.; Shahabuddin, S.; Ahmed, M. S.; Pandey, A. *Solar Energy* **2018**, *174*, 1097-1125.

[3] Wu, J.; Lan, Z.; Lin, J.; Huang, M.; Huang, Y.; Fan, L.; Luo, G.; Lin, Y.; Xiea, Y.; Weia, Y. *Chem. Soc. Rev*. **2017**, *46*, 5975-6023.

[4] Saranya, K.; Rameez, M.; Subramania, A. *Eur. Polym. J.* **2015**, *66*, 207-227.

[5] Panwar, N.; Kaushik, S.; Kothari, S. **2011**, *15*, 1513–1524.

[6] O'Brian, N.; Grübler, A.; Nakicenovic, N.; Obersteiner, M.; Riahi, K.; Schrattenholzer, L.; Toth, F. *Science* **2003**, *300*, 581–584.

[7] Chopra, K.; Paulson, P.; Dutta, V. *Prog. Photovoltaics Res. Appl*. **2004**, *12*, 69–92.

[8] Green, M. A. In Photovoltaics: coming of age, Proceedings of the IEEE Conference on Photovoltaic Specialists, Kissimmee, FL, USA, 1990, pp. 1-8.

[9] Green, M.A.; Hishikawa, Y.; Dunlop, E.D.; Levi, D.H.; Hohl-Ebinger, J.; Ho-Baillie, A.W.Y. *Prog. Photovoltaics Res. Appl.* **2018**, *26*, 3–12.

[10] Li, Q.; Wu, J.; Tang, Q.; Lan, Z.; Li, P.; Lin, J.; Fan, L. *Electrochem. commun*. 2008, 10, 1299–1302.

[11] Narudin, N.; Ekanayake, P.; Soon, Y. W.; Nakajima, H.; Lim, C. M. *Sol. Energy* **2021**, *225*, 237-244.

[12] Sen, A.; Putra, M. H.; Biswas, A. K.; Behera, A. K.; Gro, A. *Dyes Pigm.* **2023**, *213*, 111087.

[13] Yeoh, M.E.; Jaloman, A.; Chan K.Y. *Microelectron. Int.* **2019**, *36*, 68–72.

[14] Kabir, F.; NazmusSakib, S.; Shehab-Uddin, S.; TawsifEfaz, E.; Farhan-Himel M.T. *Sustain. Energy Technol. Assess.* **2019**, 35, 298–307.

[15] Fakharuddin, A.; Jose, R.; Brown, T.M.; Fabregat-Santiago, F.; Bisquert, J. *Energy Environ Sci.* **2014**, *7*, 3952-3981.

[16] Jung, H.S.; Park N-G. *Small* 2015, *11*, 10–25.

[17] Zuo, C.; Bolink, H.J.; Han, H.; Huang, J.; Cahen, D.; Ding, L. *Adv. Sci.* **2016**, 3, 1500324.

[18] Ono, L.K.; Leyden, M.R.; Wang, S.; Qi, Y. *J. Mater. Chem.* A **2016**, *4*, 6693–6713.

[19] Jung, H.S.; Park N-G. *Small* **2015**, *11*, 10–25.

[20] Jennings, J.R.; Liu, Y.; Wang, Q. *J. Phys. Chem. C* **2011**, *115*, 15109–15120.

[21] Chiba, Y.; Islam, A.; Watanabe, Y.; Komiya, R.; Koide, N.; Han, L. *J. Appl. Phys.* **2006**, *45*, 638–640.

[22] Koo, H-J.; Kim, Y.J.; Lee, Y.H.; Lee, W.I,; Kim, K.; Park, N-G. *Adv. Mater* **2008**, *20*,195–199.

[23] Maçaira, J.; Andrade, L.; Mendes, A. *Sol Energy* **2017**, *158*, 905–916.

[24] Chandiran, A.K.; Casas-Cabanas, M.; Comte, P.; Zakeeruddin, S.M.; Graetzel, M. *J. Phys. Chem C* **2010**, *114*, 15849–15856.

[25] Yu, J.; Yang, Y.; Fan, R.; Liu, D.; Wei, L.; Chen, S.; Li, L.; Yang, B.; Cao, W. *Inorg.Chem.* **2014**, *53*, 8045–8053.

[26] Vittal, R.; Ho, K.C. Renew Sustain Energy Rev. **2017**, *70*, 920–935.

[27] Birkel, A.; Lee, Y-G.; Koll, D.; Van Meerbeek, X.; Frank, S.; Choi, M. J.; Kang, Y. S.; Char, K.; Tremel, W. *Energy Environ. Sci.* **2012**, *5*, 5392-5400.

[28] Manikandan, A.; Saravanan, A.; Antony, S.A.; Bououdina, M. *J. Nanosci. Nanotechnol*. **2014**, *15*, 4358–4366.

[29] Ghosh, R.; Brennaman, M.K.; Uher, T.; Ok. M.R.; Samulski, E.T.; McNeil L.E.; Meyer. T.J.; Lopez, R. *ACS Appl. Mater. Interfaces* **2011**, *3*, 3929–3935

[30] Baghel, S.; Jha, R.; Jindal, N. *Renew. Energy* **2014**, *2*, 7.

[31] O'Regan, B.; Gratzel, M. *Nature* **1991**, *353*, 737–740.

[32] Nazeeruddin, M.K.; P´echy, P.; Renouard, T.; Zakeeruddin S.M.; Humphry-Baker, R.; Cointe, P.; Liska, P.; Cevey, L.; Costa, E.; Shklover, V.; Spiccia, L.; Deacon, G.B.; Bignozzi, C.A.; Gratzel, M. *J. Am. Chem. Soc.* **2001**, *123*, 1613–1624.

[33] Gao, F.; Wang, Y.; Shi, D.; Zhang, J.; Wang, M.; Jing, X.; Humphry-Baker, R.; Wang, P.; Zakeeruddin, SM.; Gratzel, M. *J. Am. Chem. Soc.* **2008**, *130*, 10720.

[34] Wang, S.W.; Chou, C.C.; Hu, F.C.; Wu, K.L.; Chi, Y.; Clifford, J.N.; Palomares, E.; Liu, S.H.; Chou, P.T.; Wei, T.C.; Hsiao, T.Y. *J. Mater. Chem. A* **2014**, *2*, 17618–17627.

[35] Numata, Y.; Singh, S.P.; Islam, A.; Iwamura, M.; Imai, A.; Nozaki, K.; Han, L. Adv. *Funct. Mater.* **2013**, *23*, 1817–1823.

[36] Kohle, O.; Gratzel, M.; Meyer, A.F.; Meyer, T.B. *Adv. Mater.* **1997**, *9*, 904–906.

[37] Emsley, J. In *Nature's building blocks*: *an A-Z guide to the elements*, 2nd ed.; Oxford University Press; 2011.

[38] Zhang, S.; Yang, X.; Numata, Y.; Han, L. *Energy Environ. Sci.* **2013**, *6*, 1443–1464

[39] Ezhumalai, Y.; Lee, B.; Fan, M. S.; Harutyunyan, B.; Prabakaran, K.; Lee, C. P.; Chang, S. H.; Ni, J. S.; Vegiraju, S.; Priyanka, P.; Wu, Y. W.; Liu. C.W.; Yau, S.; Lin, J. T.; Wu, C. G.; Bedzyk, M.J.; Chang, R. P. H.; Chen, M. C.; Ho, K. C.; Marks, T. J. *J. Mater. Chem. A* **2017**, *5*, 12310–12321.

[40] Ito, S.; Miura, H.; Uchida, S.; Takata, M.; Sumioka, K.; Liska, P.; Comte, P.; P´echy, P.; Gratzel, M. *Chem. Commun.* **2008**, 5194–5196.

[41] Yao, Z.; Zhang, M; Wu, H.; Yang, L.; Li, R.; Wang, P. *J. Am. Chem. Soc.* **2015**, *137*, 3799–3802.

[42] Hua, Y..; Lee, L. T. L.; Zhang, C.; Zhao, J.; Chen, T.; Wong, W. Y.; Wong, W. K.; Zhu, X. *J. Mater. Chem. A* **2015**, *3*, 13848–13855.

[43] Mariotti, N.; Gerbaldi, C.; Bonomo, M.; Bella, F.; Fagiolari, L.; Barbero, N.; Barolo, C. *Green Chem.* **2020**, *22*, 7168–7218.

[44] Mariotti, N.; Bonomo, M.; Barolo, C. In *Criticisms and Potential Improvements, Reliability and Ecological Aspects of Photovoltaic Modules*; Eds. A. Gok, IntechOpen, London, 2020.

[45] Bella, F.; Ozzello, E. D.; Sacco, A.; Bianco, S.; Bongiovanni, R. *Int. J. Hydrog. Energy* **2014**, *39*, 3036– 3045.

[46] Bella, F.; Popovic, J.; Lamberti, A.; Tresso, E.; Gerbaldi, C.; Maier, J. *ACS Appl. Mater. Interfaces*, **2017**, *9*, 37797–37803.

[47] Benesperi, I.; Michaels, H.; Freitag, M. *J. Mater. Chem. C* **2018**, *6*, 11903–11942.

[48] Gong, J.; Liang, J.; Sumathy, K. *Renewable Sustainable Energy Rev.* **2012**, *16*, 5848–5860.

[49] Cobalt Institute, https://www.cobaltinstitute.org/, (accessed 2023-03-19).

[50] Banerjee, A.; Upadhyay, K.K.; Bhatnagar, S.; Tathavadekar, M.; Bansode, U.; Agarkar, S.; Satishchandra B. O. *RSC Adv.* **2014**, *4*, 8289–8294.

[51] Neves, S.; Polo-Fonseca, C. *J. Power Sources* **2002**, *107*, 13-17.

[52] Chiang, C.; Fincher, C.; Park, Y.; Heeger, A.; Shirakawa, H.; Louis, E.; Gau, S.; MacDiarmid, A. *Phys. Rev. Lett.* **1977**, *39*, 1098–1101.

[53]Shirakawa, H.; Louis, E.; MacDiarmid, A.; Chiang, C.; Heeger, A. *Chem. Commun.***1977**, 578–580.

[54] Kirchmeyer, S.; Reuter, K. *J. Mater. Chem.* **2005**, *15*, 2077–2088

[55] Groenendaal, L.; Jonas, F.; Freitag, D.; Pielartzik, H.; Reynolds, J. *Adv. Mater.* **2000**, *12*, 481–494.

[56] Jonas, F.; Schrader, L. Synth. Met.1991, 41, 831–836.

[57] Heywang, G.; Jonas, F. *Adv. Mater.* **1992**, *4*, 116–118.

[58] Jonas, F.; Krafft, W.; Muys, B. Poly(3, 4-ethylenedioxythiophene): Conductive coatings, technical applications and properties. *Macromol Symp*. **1995**, *100*, 169–173.

[59] Po, R.; Carbonera, C.; Bernardi, A.; Tinti, F.; Camaioni, N. *Sol. Energy Mater. Sol. Cells* **2012**, *100*, 97–114.

[60] Sondergaard, R.; Hosel, M.; Angmo, D.; Larsen-Olsen, T.; Krebs, F. *Mater. Today*, **2012**, *15*, 36–49.

[61] Y. Saito, T. Kitamura, Y. Wada and S. Yanagida, Chem. Lett., 2002, 1060–1061

[62] Pringle, J.; Armel, V.; MacFarlane, D. *Chem. Commun.* **2010**, *46*, 5367–5369.

[63] Ahmad, S.; Yum, J.; Xianxi, Z.; Gratzel, M.; Butt, H.; Nazeeruddin, M. *J. Mater. Chem.* **2010**, *20*, 1654–1658

[64] Trevisan, R.; Dobbelin, M.; Boix, P.; Barea, E.; Tena-Zaera, R.; Mora-Sero, B. *Adv. Energy Mater.* **2011**, *1*, 781–784.

[65] Lee, T.; Do, K.; Lee, Y.; Jeon, S.; Kim, C.; Ko, J.; Im, S. *J. Mater. Chem.* **2012**, *22*, 21624–21629.

[66] Ahmad, S.; Bessho, T.; Kessler, F.; Baranoff, E.; Frey, J.; Yi, C.; Gratzel, M.; Nazeeruddin, M. *Phys. Chem. Chem. Phys*. **2012**, *14*, 10631–10639.

[67] Tsao, H.; Burschka, J.; Yi, C.; Kessler, F.; Nazeeruddin, M.; Gratzel, M. *Energy Environ. Sci.* **2011**, *4*, 4921–4924.

[68] Burschka, J.; Brault, V.; Ahmad, S.; Breau, L.; Nazeeruddin, M.; Marsan, B.; Zakeeruddin, S.; Gratzel, M. *Energy Environ. Sci*. **2012**, *5*, 6089–6097.

[69] Lee, K.; Chen, P.; Hsu, C.; Huang, J.; Ho, W.; Chen, H.; Ho, K. *J. Power Sources* **2009**, *188*, 313–318.

[70] Ahmad, S.; Yum, J.; Butt, H.; M. Nazeeruddin and M. Gratzel, ChemPhysChem, **2010**, *11*, 2814–2819.

[71] Yum, J.; Baranoff, E.; Kessler, F.; Moehl, T.; Ahmad, S.; Bessho, T.; Mar-chioro, A.; Ghadiri, E.; Moser, J.; Yi, C.; Nazeeruddin, M.; Gratzel, M. *Nat. Commun.* **2012**, *3*, 631–638.

[72] Amasawa, E.; Sasagawa, N.; Kimura, M.; Taya, M. *Adv. Energy Mater*. **2014**, *4*, 1400379.

[73] MacDiarmid, A. *Angew. Chem. Int. Ed.* **2001**, *40*, 2581–2590.

[74] Letheby, H. *J. Chem. Soc.* **1862**, *15*, 161–163.

[75] Chiang, J.; MacDiarmid, A. *Synth. Met.* **1986**, *1*, 193–205.

[76] Heeger, A. *Rev. Mod. Phys.* **2001**, *73*, 681–700.

[77] Wu, G.; More, K.; Johnston, C.; Zelenay, P. *Science* **2011**, *332*, 443–447.

[78] Wu, C.; Bein, T. *Science* **1994**, *264*, 1757–1759.

[79] Bhadra, S.; Khastgir, D.; Singha, N.; Lee, J. *Prog. Polym. Sci.* **2009**, *34*, 783–810.

[80] Stejskal, J.; Gilbert, R. *Pure Appl. Chem.* **2002**, *74*, 857–867.

[81] Syed, A.; Dinesan, M.; *Talanta*, **1991**, *38*, 815–837

[82] MacDiarmid, A. *Angew. Chem.* **2001**, *113*, 2649–2659.

[83] Kang, E.; Neoh, K.; Tan, K. *Prog. Polym. Sci.* **1998**, *23*, 277–324

[84] Li, Q.; Wu, J.; Tang, Q.; Lan, Z.; Li, P.; Lin, J.; Fan, L. *Electrochem. Commun.* **2008**, *10*, 1299–1302

[85] Wang, H.; Feng, Q.; Gong, F.; Li, Y.; Zhou, G.; Wang, Z. *J. Mater. Chem. A* **2013**, *1*, 97–104.

[86] Hou, W.; Xiao, Y.; Han, G.; Fu, D.; Wu, R. *J. Power Sources* **2016**, *322*, 155–162

[87] Tai, Q.; Chen, B.; Guo, F.; Xu, S.; Hu, H.; Sebo, B.; Zhao, X. *ACS Nano*. **2011**, *5*, 3795–3799

[88] Wu, J.; Li, Y.; Tang, Q.; Yue, G.; Lin, J.; Huang, M.; Meng, L. *Sci. Rep.* **2014**, *4*, 4028.

[89] Saito, Y.; Kubo, W.; Kitamura, T.; Wada, Y.; Yanagida, S. *J. Photochem. Photobiol*. A **2004**, *164*, 153–157.

[90] Xia, J.; Masaki, N.; Jiang, K.; Yanagida, S. *J. Mater. Chem.* **2007**, *17*, 2845–2850.

[91] Li, Z.; Ye, B.; Hu, X.; Ma, X.; Zhang, X.; Deng, Y. *Electrochem. Commun.* **2009**, *11*, 1768–1771

[92] Qiu, Y.; Lu, S.; Wang, S.; Zhang, X.; He, S.; He, T. *J. Power Sources*, **2014**, *253*, 300–304

[93] Chiang, C.; Chen, S.; Wu, C.; *Org. Electron.* **2013**, *14*, 2369–2378.

[94] Yun, S.; Hagfeldt, A.; Ma, T. *Adv. Mater.* **2014**, *26*, 6210–6237.

[95] McNeill, R.; Siudak, R.; Wardlaw, J.; Weiss, D. *Aust. J. Chem.* **1963**, *16*, 1056–1075

[96] Vernitskaya, T.; Efimov, O.; *Russ. Chem. Rev*. **1997**, *66*, 443–457.

[97] Xia, J.; Chen, L.; Yanagida, S. *J. Mater. Chem.* **2011**, *21*, 4644–4649.

[98] Jeon, S.; Kim, C.; Ko, J.; Im, S. *J. Mater. Chem.* **2011**, *21*, 8146–8151.

[99] Janata, J.; JosowiCbz, M. *Nat. Mater.* **2003**, *2*, 19–24.

[100] Huang, Y.; Li, H.; Wang, Z.; Zhu, M.; Pei, Z.; Xue, Q.; Huang, Y.; Zhi, C. *Nano Energy*, **2016**, *22*, 422–438.

[101] Zhang, X.; Zhang, J.; Song, W.; Liu, Z. *J. Phys. Chem. B* **2006**, *110*, 1158–1165

[102] Wu, J.; Li, Q.; Fan, L.; Lan, Z.; Li, P.; Lin, J.; Hao, S.; *J. Power Sources* **2008**, *181*, 172–176.

[103] Peng, T.; Sun, W.; Huang, C.; Yu, W.; Sebo, B.; Dai, Z.; Guom, S.; Zhao, X. *ACS Appl. Mater. Interfaces* **2014**, *6*, 14–17.

[104] Hwang, D.; Song, D.; Jeon, S.; Han, T.; Kang, Y.; Im, S. *J. Mater. Chem. A* **2014**, *2*, 859–865.

[105] Kitamura, T.; Maitani, M.; Matsuda, M.; Wada, Y.; Yanagida, S. *Chem. Lett.* **2001**, 1054–1055.

[106] Cervini, R.; Cheng, Y.; Simon, G. *J. Phys. D: Appl. Phys.* **2004**, *37*, 13–20.

[107] Kang, E.; Tan, T.; Neoh, K.; Ong, Y. *Polymer* **1986**, *27*, 1958–1962.

[108] Lu, S.; Wang, S.; Han, R.; Feng, T.; Guo, L.; Zhang, X.; Liu, D.; He, T. *J. Mater. Chem. A* **2014**, *2*, 12805–12811.

[109] Makris, T.; Dracopoulos, V.; Stergiopoulos, T.; Lianos, P. *Electrochim. Acta* **2011**, *56*, 2004–2008.

[110] Zhang, X.; Wang, S.; Lu, S.; Su, J.; He, T. *J. Power Sources* **2014**, *246*, 491–498.

[111] Keothongkham, K.; Pimanpang, S.; Maiaugree, W.; Saekow, S.; Jarernboon, W.; Amornkitbamrung, V. *Int. J. Photoenergy* **2012**, *67*, 1326.

[112] Veerender, P.; Saxena, V.; Jha, P.; Koiry, S.; Gusain, A.; Samanta, S.; Chauhan, A.; Aswal, D.; Gupta, S. *Org. Electron.* **2012**, *13*, 3032–3039.

[113] Xu, J.; Li, M.; Wu, L.; Sun, Y.; Zhu, L.; Gu, S.; Liu, L.; Bai, Z.; Fang, D.; Xu, W. *J. Power Sources* **2014**, *257*, 230–236.

[114] Bu, C.; Tai, Q.; Liu, Y.; Guo, S.; Zhao, X.; *J. Power Sources* **2013**, *221*, 78–83.

[115] Theerthagiri, J.; Senthil, A.; Madhavan, J.; Maiyalagan, T. *ChemElectroChem* **2015**, *2*, 928–945.

[116] Xu, H.; Zhang, X.; Zhang, C.; Liu, Z.; Zhou, X.; Pang, S.; Chen, X.; Dong, S.; Zhang, Z.; Zhang, L.; Han, P.; Wang, X.; Cui, G. *ACS Appl. Mater. Interfaces* **2012**, 4, 1087.

[117] Yeh, M. H.; Lin, L. Y.; Lee, C. P.; Wei, H. Y.; Chen, C. Y.; Wu, C. G.; Vittal, R.; Ho, K. C. *J. Mater. Chem.* **2011**, *21*, 19021–19029

[118] Fan, B.; Mei, X.; Sun, K.; Ouyang, J. *Appl. Phys. Lett.* **2008**, *93*, 143101–143103.

[119] Chen, J. G.; Wei, H. Y.; Ho, K. C. *Sol. Energy Mater. Sol. Cells* **2007**, *91*, 1472–1477.

[120] Hong, W.; Xu, Y.; Lu, G.; Li, C.; Shi, G. *Electrochem Commun* **2008**, *10*, 1555–1558.

[121] Kitamura, K.; Shiratori, S. *Nanotechnology* **2011**, *22*, 195703–195709.

[122] Yue, G.; Wu, J.; Xiao, Y.; Lin, J.; Huang, M. *Electrochim. Acta* **2012**, 67, 113–121.

[123] Sudhagar, P.; Nagarajan, S.; Lee, Y. G.; Song, D.; Son, T.; Cho, W.; Heo, M.; Lee, K.; Won, J.; Kang, Y. S. *ACS Appl. Mater. Interfaces* **2011**, *3*, 1838–1843.

[124] Yeh, M, H.; Lee, C. P.; Lin, L. Y.; Nien, P. C.; Chen, P. Y.; Vittal, R.; Ho, K. C. *Electrochim. Acta* **2011**, *56*, 6157–6164.

[125] Wang, H.; Wei, W.; Hu, Y. *Top. Catal.* **2013**, 1–5.

[126] Xiao, Y.; Wu, J.; Lin, J. Y.; Yue, G.; Lin, J.; Huang, M.; Lan, Z.; Fan, L. *J Power Sources* **2013**, *241*, 373–378.

[127] Chen, J.; Li, B.; Zheng, J.; Zhao, J.; Jing, H.; Zhu, Z. *Electrochim. Acta* **2011**, *56*, 4624–4630.

[128] Peng, S.; Wu, Y.; Zhu, P.; Thavasi, V.; Mhaisalka,r S. G.; Ramakrishna, S. *J. Photochem. Photobiol*. *A* **2011**, *223*, 97–102.

[129] Shin, H. J.; Jeon, S. S.; Im, S.S. *Synth. Met.* **2011**, *161*, 1284–1288.

[130] Wang, G.; Xing, W.; Zhuo, S. *Electrochim. Acta* **2012**, *66*, 151–157.

[131] Peng, S.; Tian, L.; Liang, J.; Mhaisalkar, S. G.; Ramakrishna, S. *ACS Appl. Mater. Interfaces* **2012**, *4*, 397–404.

[132] Zhang, J.; Long, H.; Miralles, S. G.; Bisquert, J.; Fabregat-Santiago, F.; Zhang, M. *Phys. Chem. Chem. Phys.* **2012**, 14, 7131–7136.

[133] Gong, F.; Xu, X.; Zhou, G.; Wang, Z. S. *Phys. Chem. Chem. Phys.* **2013**, *15*, 546–52.

[134] Yue, G. T.; Wu, J. H.; Xiao, Y. M.; Lin, J. M.; Huang, M. L.; Lan, Z. *J. Phys. Chem. C* **2012**, *116*, 18057–18063.

[135] Xiao, Y.; Lin, J. Y.; Wu, J.; Tai, S. Y.; Yue, G.; Lin, T. W. *J. Power Sources* **2013**, *233*, 320–325.

[136] Hauch, A.; Georg, A. *Electrochim. Acta* **2001**, *46*, 3457–66.

[137] Yun. S.; Wang, L.; Guo, W.; Ma, T. *Electrochem. Commun*. **2012**, *24*, 69–73.

[138] Lin, X,; Wu, M.; Wang, Y.; Hagfeldt, A.; Ma, T. *Chem. Commun*. **2011**, *47*, 11489–11491.

[139] Ramasamy, E.; Jo, C.; Anthonysamy, A.; Jeong, I.; Kim, J.; Lee, K. *J. Chem. Mater*. **2012**, *24*, 1575–1582.

[140] Yun, S.; Hagfeldt, A.; Ma, T. *Adv. Mater* **2014**, 26, 6210–6237.

[141] Yun, S.; Zhang, H.; Pu, H.; Chen, J.; Hagfeldt, A.; Ma, T. *Adv. Energy Mater*. **2013**, *3*, 1407–1412

[142] Wang, G.; Xing, W.; Zhuo, S. *J. Power Sources* **2009**, *194*, 568–573.

[143] Yun, S.; Pu, H.; Chen, J.; Hagfeldt, A.; Ma, T. *ChemSusChem* **2014**, *7*, 442–450.

[144] Bennett, L. H.; Cuthill, J. R.; McAlister, A. J.; Erickson, N. E.; Watson, R. E. *Science* **1974**, *184*, 563–565.

[145] Colton, R. J.; Rabalais, J. W. *Inorg. Chem.* **1976**, *15*, 236–268.

[146] Oyama, S. T. *Catal. Today* **1992**, 15, 179–200.

[147] Furimsky, E. *Appl. Catal. A Gen.* **2003**, *240*, 1–28.

[148] Thomas, S.; Deepak, T. G.; Anjusree, G. S.; Arun TA, Nair SV, Nair AS. *J. Mater. Chem A* 2014;2:4474–90.

[149] Yun, S.; Wu, M.; Wang, Y.; Shi, J.; Lin, X.; Hagfeldt, A.; Ma, T. *ChemSusChem* **2013,** 6, 411–6.

[150] Jeon, S.S.; Kim, C.; Ko, J.; Im, S.S. *J. Mater. Chem.* **2011**, *21*, 8146–51.

[151] Trevisan, R.; Döbbelin, M.; Boix, P. P.; Barea, E. M.; Tena-Zaera, R.; Mora-Seró, I.; Bisquert, J. *Adv Energy Mater* **2011**, *1*,781–4.

[152] Lee, T. H.; Do, K.; Lee, Y. W.; Jeon, S. S.; Kim, C.; Ko, J. Im, S. S. *J. Mater. Chem.* **2012**, *22*, 21624–21629

[153] Wang, H.; Feng, Q.; Gong, F.; Li, Y.; Zhou, G.; Wang, Z. S. *J. Mater. Chem. A* 2013;1:97–104.

[154] Wu, M.; Lin, X.; Hagfeldt, A.; Ma, T. *Chem. Commun 2011*, 47, 4535–4537.

[155] Yun, S. Freitas, J. N.; Ana, F.; Nogueira, C.; Wang, Y.; Ahmad, S.; Wang, Z-S. *Prog. Poly. Sci.* **2016**, *59*, 1–40.

[156] Zhou, W.; Apkarian, R. P.; Wang, Z. L. Scanning Microscopy for Nanotechnology, Springer, 2007.

[157] Pazoki, M. Cappel, U. B.; Erik, M.; Johansson, J.; Hagfeldt, A.; Boschloo, G. *Energy Environ. Sci.* **2017**, *10*, 672.

[158] Thomas, S.; Deepak, T. G.; Anjusree, G. S.; Arun, T. A.; Nair, S. V.; Nair, A. S. *J. Mater. Chem. A* **2014**, *2*, 4474–4490.

[159] Zhang, Q.; Cao, G. *Nano. Today* **2011**, *6*, 91–106.

[160] Snaith, H. J.; Schmidt-Mende, L. *Adv. Mater.* **2007**, *19*, 3187–3200.

[161] Ellis, H.; Vlachopoulos, N.; Haggman, L. Perruchot, C.; Jouini, M.; Boschloo, G.; Hagfeldt, A. *Electrochim. Acta* **2013**, *107*, 45–51.

[162] Chung, I.; Lee, B.; He, J.; Chang, R. P. H.; Kanatzidis, M. G. *Nature*, **2012**, *485*, 486–489

[163] Lee, K.; Park, S. W.; Ko, M. J.; Kim, K.; Park, N. *Nat. Mater.* **2009**, *8*, 665–671.

[164] Liu, R.; Qiang, L.; Yang, W.; Liu, H. *J. Power Sources* **2013**, *223*, 254–258

[165] Schmidt-Mende, L.; Gratzel, M. *Thin Solid Films* **2006**, *500*, 296–301.

[166] Cappel, U. B.; Gibson, E. A.; Hagfeldt, A.; Boschloo, G. *J. Phys. Chem. C*, **2009**, *113*, 6275–6281.

[167] Ding, I.-K.; Te´treault, N.; Brillet, J.; Hardin, E.; Smith, E.; Rosenthal, H.; Sauvage, F.; Gra¨tzel, M.; McGehee, M. D. *Adv. Funct. Mater.* **2009**, *19*, 2431–2436.

[168] Docampo, P.; Hey, A.; Guldin, S.; Gunning, R.; Steiner, U.; Snaith, H. J. *Adv. Funct. Mater.* **2012**, *22*, 5010–5019.

[169] Seeck, O. H. In X-Ray Diffraction: Modern Experimental Techniques, ed. B. Murphy, Pan Stanford, 2015.

[170] Wang, L.; Al-Mamun, M.; Liu, P.; Wang, Y.; Yang, H. G.; Wang, H. F.; Zhao, H. *NPG Asia Mater.* **2015**, *7*, 226.

[171] Josefsson, I.; Eriksson, S. K.; Ottosson, N.; O¨hrwall, G.; Siegbahn, H.; Hagfeldt, A.; Rensmo, H.; Bjo¨rneholm, O.; Odelius, M. *Phys. Chem. Chem. Phys.* **2013**, *15*, 20189–20196.

[172] Shi, Z.; Deng, K.; Li, L. *Sci. Rep.* **2015**, *5*, 9317.

[173] Fantacci, S.; De Angelis, F. *Coord. Chem. Rev.* **2011**, *255*, 2704–2726.

[174] Mishra, A.; Fischer, M.; Bauerle, P. *Angew. Chem.* **2009**, *48*, 2474–2499.

[175] Ondersma, J.; Hamann, T. *Coord. Chem. Rev.*, **2013**, 257, 1533–1543.

[176] Listorti, A.; O'Regan, B.; Durrant, J. *Chem. Mater.* ***2011***, *23*, 3381–3399.

[176] Dunn, H.; Peter, L. *J. Phys. Chem. C* **2009**, *113*, 4726–4731.

[177] Liu, W.; Hu, L.; Huo, Z.; Dai, S. *Prog. Chem.* **2009**, *21*, 1085–1093.

[178] Bard, A. J.; Faulkner, L. R. Electrochemical Methods: Fundamentals and Applications, John Wiley and Sons Inc., New York, 2001

[179] Park, B.; Pazoki, M.; Aitola, K.; Jeong, S.; Johansson, E. M. J.; Hagfeldt, A.; Boschloo, G. *ACS Appl. Mater. Interfaces* **2014**, *6*, 2074–2079.

[180] Fabregat-Santiago, F.; Bisquert, J.; Cevey, L.; Chen, P.; Wang, M.; Zakeeruddin, S.; Gratzel, M. *J. Am. Chem. Soc.* **2008**, *131*, 558–562.

[181] Han, L.; Koide, N.; Chiba, Y.; Islam, A.; Komiya, R.; Nobuhiro, F.; Fukui, A. Yamanaka, R. *Appl. Phys. Lett.* **2005**, *86*, 213501.

[182] Wang, Q.; Moser, J.; Gra1tzel, M. *J. Phys. Chem. B* **2005**, *109*, 14945–14953.

[183] Huang, Z.; Natu, G.; Ji, Z.; Hasin, P.; Wu, Y. *J. Phys. Chem. C* **2011**, *115*, 25109–25114

[183] Liu, W.; Kou, D.; Cai, M.; Hu, L.; Dai, S. *Prog. Chem.* **2012**, *24*, 722–736

[184] Yin, J.; Bing, Q.; Wang, L.; Wang, G. *Acta A Mol. Biomol. Spectrosc*. **2018**, *189*, 495–501.

[185] Baptayev, B.; Tashenov, Y.; Aliakbarova, A.; Adilov, S.; Balanay, M. *Materials Today: Proceedings* **2022**.

[186] Akbayrak, M.; Cansu-Ergun, E. G.; Önal, A. M. *Des Monomers Polym*. **2016**, *19*, 679-687.

[187] Elham, N. B.; Reda, M. E-S. Efficient Synthesis of Formyl Boronate Esters Derived from Carbazole and Phenoxazine as Key Electron Donors. Polycycl. Aromat. Compd. **2022**, *42 (10)*, 7178-7186.